Morphogenesis, cell movement and phagocytosis are driven by dynamic reorganization of the actin cytoskeleton[13,14]. We showed previously that activation of $P2Y_{12/13}$ receptors, another microglial G-protein-coupled receptor, resulted in membrane ruffling and chemotaxis in microglia[5,6], and therefore we sought first to determine whether the $P2Y_6$-receptor-mediated signals affect the cell movement of microglia. Membrane ruffles are structures that are found primarily at the front edges of migrating cells[15]. To determine whether $P2Y_6$ activation stimulates microglial chemotaxis, cells were stimulated with either UDP or ATP. Neither lamellipodia-like membrane ruffles (Fig. 2a left) nor chemotaxis (Fig. 2b left) were observed when stimulated with UDP, whereas ATP produced both responses (Fig. 2a right and Fig. 2b right). However, UDP caused actin reorganization and formed aggregates of F-actin in the interior of the cells (Fig. 2a left, arrows). On stimulation with UDP (100 μM), microglia rapidly changed their morphology (Supplementary Fig. 2a); namely, to microglial processes with filopodia-like protrusions (arrows) and phagosome-like vacuoles (arrowheads). A crown-like circular structure rich in F-actins, termed the 'phagocytotic cup'[16], was also observed around the zymosan particles (Supplementary Fig. 2b, red). We speculated that UDP somehow regulates the morphogenesis of microglia, which may be involved in microglial endocytotic activities such as pinocytosis, macropinocytosis and phagocytosis. Phagocytosis is one of the most important physiological functions of microglia[17] and is the process activating the uptake of larger particles (more than 0.5 μm) by actin-based mechanisms. We investigated the UDP-evoked phagocytosis process by time-lapse videomicroscopy and flow cytometry (fluorescence-activated cell sorting; FACS)-based assay. When stimulated with 100 μM UDP, microglia rapidly phagocytosed fluorescent zymosan particles (green) (Fig. 2c, see also Supplementary Video). A quantitative phagocytosis assay by FACS shows that UDP induced the phagocytosis of latex beads in a concentration-dependent fashion (5–1,000 μM) in a 20-min incubation period (Fig. 2d). GDP (100–1,000 μM), a weak agonist of the $P2Y_6$ receptor, caused a slight uptake of microspheres (at 100 μM this was 49.7 ± 8.6% of UDP alone; $n = 4$) but ADP, also known as a weak partial agonist of the mouse $P2Y_6$ receptor, failed to stimulate the uptake (at 100 μM it was 0.3 ± 2.3% of UDP alone; $n = 4$). This is in good agreement with the previous finding that ADP does not activate rat $P2Y_6$ receptors[18]. The phagocytosis induced by 100 μM UDP was significantly inhibited by 30–100 μM RB2, a higher concentration of suramin (300 μM) and MRS2578 (0.01–3 μM), and was nearly abolished by $P2Y_6$ AS (Fig. 2e; see also Supplementary Fig. 2c, d). Recent reports indicate the existence of functional cross-talk between the nucleotides and cysteinyl leukotrienes (CysLTs, for example LTD4) in orchestrating inflammatory responses[19], indicating that some nucleotides may reveal their functions by means of a CysLT receptor (CysLTR). Microglia express a functional CysLT1R, whose activation by LTD4 resulted in an increase in $[Ca^{2+}]_i$ in microglia (Supplementary Fig. 3a). Thus, UDP acting on CysLT1R may reveal various microglial responses. However, MRS2578, a selective $P2Y_6$ receptor antagonist, did not block the LTD4-evoked Ca^{2+} responses in CysLT1R-transfected Chinese hamster ovary cells (Supplementary Fig. 3b) at a dose that inhibited the UDP-evoked increase in $[Ca^{2+}]_i$ and phagocytosis in microglia (Figs 1c and 2e). In addition, 1 μM LTD4 did not induce phagocytosis in microglia (Supplementary Fig. 3c, 4.8 ± 4.2% of that with 100 μM UDP alone; $n = 3$). All these findings suggest that the contribution of the CysLT1R to the UDP-evoked phagocytosis in microglia is negligible. Taken together, these data strongly suggest that rat microglial $P2Y_6$ receptors are coupled with phagocytic functions. The UDP-evoked phagocytosis was inhibited by 1 μM thapsigargin, the protein kinase C inhibitor staurosporin at 5 μM, and 10 μM U73122 (see Supplementary Fig. 4), indicating that activation of the $P2Y_6$ receptor seems to trigger phagocytosis through the pathway(s) mediated by PLC-linked Ca^{2+} and protein kinase C.

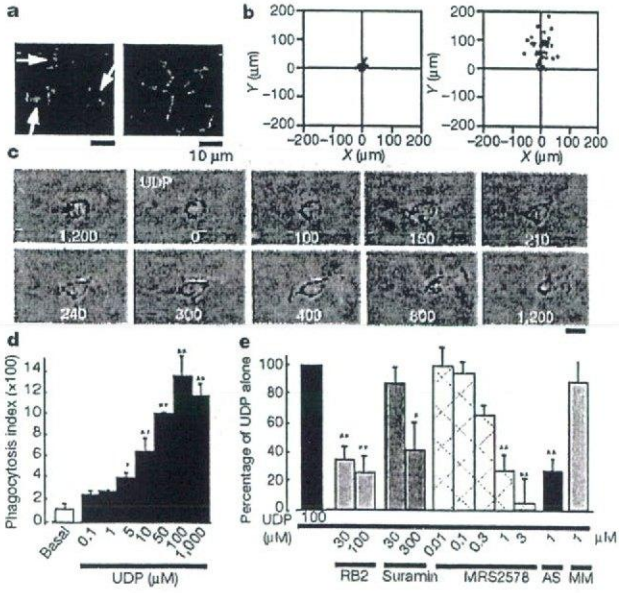

Figure 2 | Changes in cell motilities of microglia. **a**, UDP- and ATP-evoked membrane ruffles. Cultured microglia were stimulated for 5 min with 100 μM UDP (left) and 10 μM ATP (right), fixed, permeabilized, and then stained with anti-phalloidin. Scale bar, 10 μm. **b**, Typical chemotactic responses of microglia towards 100 μM UDP (left) and 100 μM ATP (right) assessed by the Dunn chemotaxis chamber (see Methods). **c**, Time-lapse images showing the effect of UDP on the microglial morphogenic changes and the uptake of fluorescent zymosan particles (green). The time after addition of UDP is shown in seconds in each picture. **d**, The UDP-evoked uptake of microspheres was assessed quantitatively as a phagocytosis index by using FACS. Data are mean and s.e.m. for three experiments (asterisk, $P < 0.05$; two asterisks, $P < 0.01$ compared with basal). **e**, Effects of the P2 receptor antagonists reactive blue 2 and suramin, the $P2Y_6$ receptor antagonist MRS2578, and $P2Y_6$ AS or MM on the UDP-evoked phagocytosis. Data are means and s.e.m. for three or four experiments (asterisk, $P < 0.05$; two asterisks, $P < 0.01$ compared with UDP alone).

Because phagocytes remove dead or damaged cells, debris and invading pathogens, recognition is the first step in phagocytosis. It is initiated by activation of the phagocytosis-promoting receptors such as Fc receptors and complement receptors[20]. In the central nervous system, microglia possess these receptors and remove amyloid-β, a key molecule in Alzheimer's disease, and attenuate Alzheimer's disease-like pathology[21]. With regard to apoptotic cells, microglia may also remove such cells by recognizing so-called 'eat-me' signals[20]. However, in the present study we used non-opsonized zymosan (Fig. 2c) and latex beads (Fig. 2d, e), which were not recognized by opsonin-dependent receptors such as Fc receptors, complement receptors or vitronectin receptors. Phagocytosis-promoting receptors also include opsonin-independent ones such as β_1-integrins, mannose receptors, scavenger receptors and phosphatidylserine receptors[13]; in fact, microglia expressed all these receptors (Supplementary Fig. 5a–e, cell lysates). Among these receptors, β_1-integrin was detected as a bead-associated protein that was slightly increased on stimulation with UDP (Supplementary Fig. 5a, bead-associated) and localized at membrane ruffle-like or phagocytic cup-like structures (see also Supplementary Fig. 2b), to which fluorescent microspheres were attached (Supplementary Fig. 5f). However, we do not know whether β_1-integrin itself binds or recognizes the microspheres. β_1-Integrin might be involved in some way in the machinery of phagocytosis or in the uptake processes of the microspheres in response to UDP, but the precise target molecule or molecules that bind or recognize microspheres to be phagocytosed remains to be identified. The microglial phagocytosis seen in the present study is a new type that is promoted by the diffusible

extracellular molecule UDP. However, we cannot deny the possibility that the UDP may simply facilitate the machinery of phagocytosis and that UDP-evoked phagocytosis observed in this study may even include macropinocytosis.

To determine the expression and function of microglial $P2Y_6$ receptors *in vivo*, the excitotoxicity of brain injury was induced by kainic acid (KA) (Fig. 3). KA is an excitatory amino acid that is often used to cause limbic motor epilepsy or excitatory neuronal cell death *in vivo* and *in vitro*. KA acts on non-NMDA glutamate receptors to facilitate excess excitability, thereby leading to necrosis and even apoptosis of neurons. The hippocampal CA1 and CA3 regions are susceptible to neuronal death in response to KA[22]. When KA was injected intraperitoneally into rats ($10\,mg\,kg^{-1}$), it produced typical limbic seizure within 60 min. At 72 h after the administration of KA, the brains were removed and were used for western blotting, immunohistochemical assays and *in situ* hybridization (ISH). Western blotting analysis showed that KA increased the expression of $P2Y_6$ receptors in comparison with the saline-injected control groups (Fig. 3A, B). Double staining of microglia and neurons by anti-Iba1 (green) and anti-neuronal nuclei (NeuN, red) antibodies, respectively, showed that KA induced severe neuronal loss in the hippocampal CA1 and CA3 regions, where intense Iba1-positive signals—indicative of microglia—were observed. KA increased the number of microglia appearing in the activated form with poorly ramified, short and thick processes (Fig. 3C, f–h). Small NeuN signals seemed to be incorporated in some microglia (see g and h in Fig. 3C), suggesting that microglia phagocytose damaged or dead neurons. These findings suggest that microglia might migrate or proliferate, probably as a result of KA-induced neuronal damage.

We further examined the cell types that produced increases in $P2Y_6$ receptor protein in response to the administration of KA, and found that $P2Y_6$ immunoreactivities (green in Fig. 3D) were associated with the microglia (OX-42, red in Fig. 3D, c) but not with astrocytes (glial fibrillary acidic protein (GFAP), red in Fig. 3D, d) or neurons (NeuN, red in Fig. 3D, e). Furthermore, we performed ISH to characterize the expression of mRNA coding for $P2Y_6$ receptors with the use of digoxigenin-labelled antisense RNA probe. Signals for $P2Y_6$ receptor mRNA were very low in the naive animals but were upregulated three days after treatment with KA (Fig. 3E, b; blue dots indicated by arrowheads). At this time, the number of microglia increased markedly, especially at the hippocampal CA3 and CA1 regions (Fig. 3C). After ISH, the sections were stained with anti-Iba1 antibody to characterize $P2Y_6$ receptor mRNA signals. In the hippocampal CA3 regions of naive rats, there were very few anti-Iba1-positive microglia that did not show $P2Y_6$ receptor mRNA. In contrast, in the hippocampal CA3 of KA-injected rats, there was an increased number of anti-Iba1-positive microglia, in which $P2Y_6$ receptor signals were colocalized with microglia (Fig. 3E, c; KA, black arrows, see also inset at higher magnification).

There is a growing literature about 'eat-me' signals that are expressed on the cell surface of apoptotic or dying cells. However, diffusible signals that trigger phagocytosis have received only limited attention. When neurons or cells are exposed to traumatic injury such as ischaemia, they swell and subsequently shrink as a result of

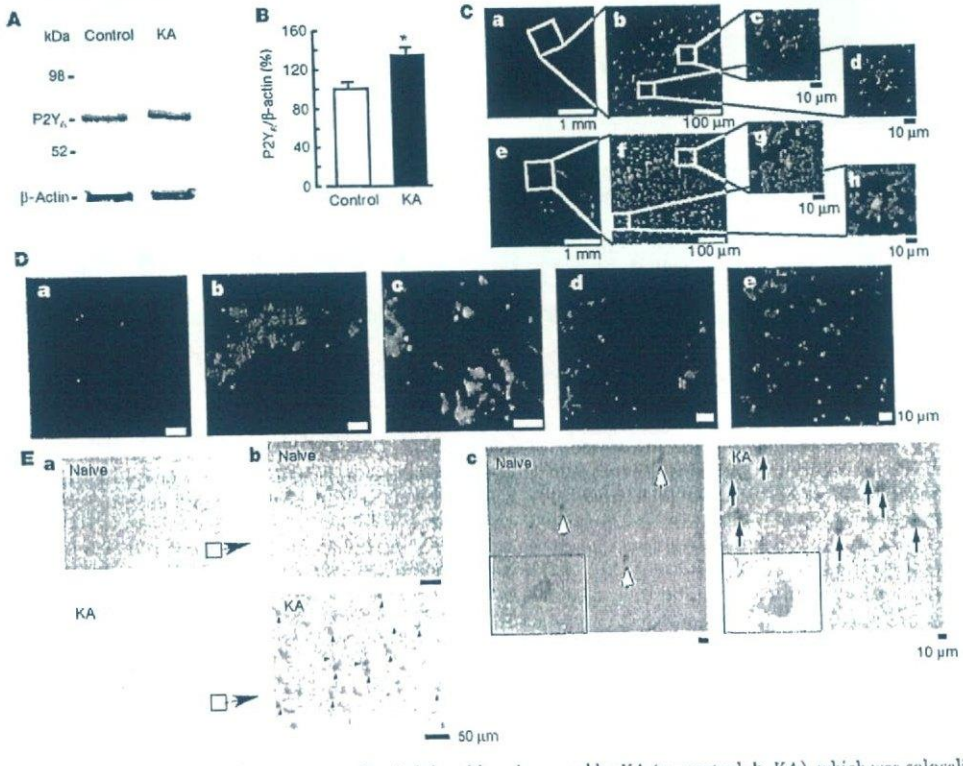

Figure 3 | Increase in $P2Y_6$ receptors in the hippocampus after kainic acid (KA)-treatment. **A**, Western blot analysis, showing increase in $P2Y_6$ receptor protein in rats treated intraperitoneally with $10\,mg\,kg^{-1}$ KA, 72 h after treatment. **B**, Summary of quantitative data; KA was applied at $10\,mg\,kg^{-1}$. Results are means and s.e.m. for 8 (control) and 7 (KA) experiments (asterisk, $P < 0.05$ compared with control). **C**, Immunohistochemical analysis in naive control (**a**–**d**) and KA-treated (**e**–**h**) rats; red, anti-NeuN antibody; green, anti-Iba1 antibody. Rectangles in **a** and **e** are expanded in **b** and **f**, respectively. Rectangles in **b** and **f** also correspond to **c**, **d** and **g**, **h**, respectively. **D**, Anti-$P2Y_6$ antibody signals (green) were increased by KA (**a**, control; **b**, KA), which was colocalized with microglia (red in **c**, anti-OX42) but not with astrocytes (red in **d**, anti-GFAP) or neurons (red in **e**, anti-NeuN). **E**, ISH analysis. **a**, **b**, mRNA coding for $P2Y_6$ receptor in naive rats was very low but was increased at the hippocampal CA3 region by KA (3 days later) (blue dots and arrowheads, KA). **c**, Double staining with $P2Y_6$ antisense RNA probe (blue dots) and anti-Iba-1 antibody (brown signals, white (naive) or black (KA) arrows). In KA-treated rats there was an increased number of microglia, which was associated with $P2Y_6$ receptor mRNA (blue signals, inset at higher magnification in KA).

increased permeability. This is followed by leakage of cytoplasmic molecules, leading to necrotic cell death. Thus, cytoplasmic nucleotides could be diffusible messengers that signal the crisis state to adjacent cells including microglia. In fact, the diffusible messenger ATP promotes microglial chemotaxis and/or migration[3–6]. Diffusible molecules might be insufficiently precise to cause phagocytes to recognize and eat cells. However, released or leaked nucleotides are immediately degraded by the extracellular nucleotide-degrading enzymes. In this respect, UDP might be a localized and transient marker of traumatized or necrotic cells.

Cell injury results in a leakage of ATP that affects the motility of adjacent cells, including microglia[3,4]. In addition, cells release or leak uridine nucleotides[23] and nucleotide sugars[24] in response to various stimuli or ischaemic injury[25]. We therefore next investigated whether KA increases the release of extracellular UDP from neurons to induce microglial phagocytosis. Cultured hippocampal neurons were stimulated with and without 100 μM KA for 1 h; the supernatant was then collected for nucleotide assay by high-performance liquid chromatography (HPLC) or for phagocytosis assay by FACS (Fig. 4). Because released or leaked UTP is rapidly degraded into UDP, UMP and uridine by ARL67156-sensitive ectonucleotidases, we monitored the amount of UTP rather than UDP, and collected the supernatant and the microdialysates in the presence of 20 μM ARL67156 throughout experiments. There was a close relationship between the HPLC peak corresponding to UTP and the concentration of the standard UTP ($R^2 = 0.9947$). The amount of UTP in the KA-treated supernatant was significantly larger than that in the KA-untreated control supernatant (Fig. 4b; control, 2.3 ± 1.1 μM; KA treated, 10.5 ± 3.9 μM, $P < 0.05$). We also tested whether the KA-treated supernatant obtained from cultured hippocampal neurons facilitated microglial phagocytosis. Hippocampal neurons were treated with and without 100 μM KA for 1 h; each supernatant was collected and added to microglia; this was followed by a phagocytosis assay. As shown in Fig. 4c, when microglia were incubated with the KA-treated supernatant for 20 min, there was a significant increase in phagocytosis, which was blocked by the $P2Y_6$ receptor antagonist MRS2578 (1 μM). KA alone did not stimulate phagocytosis.

Finally, we tested whether KA induces the release of UDP and $P2Y_6$-receptor-mediated phagocytosis *in vivo*. An increase in extracellular UTP concentration ($[UTP]_o$) was observed soon after injection of KA (from 1 to 4 h after injection), which reached 2–3-fold higher than the KA-untreated control (data not shown). At 1 day after KA injection, $[UTP]_o$ was about 1.5–2.0-fold higher than the KA-untreated control (Fig. 4e). Then, at day 3, $[UTP]_o$ reached almost 10-fold higher levels (9.4 ± 1.2-fold; Fig. 4e and inset), which decreased slightly at day 5. A higher (5–10-fold) $[UTP]_o$ was observed 2–3 days after the injection of KA, which lasted at least another couple of days. It should be noted that loss of neurons (removal of neurons) also became obvious 2–3 days after the KA injection. We further injected fluorescent microspheres into the hippocampal CA3 regions of KA-treated rats, and then counted the numbers of the microspheres phagocytosed or attached by microglia. The $P2Y_6$ receptor antagonist MRS2578 was injected into the hippocampal CA3 region, and $P2Y_6$ AS or MM (mismatch oligonucleotide) was injected into the third ventricle. The number of microspheres taken or attached by microglia was markedly increased by KA treatment, which is significantly inhibited by MRS2578 or $P2Y_6$ AS but not by MM (Fig. 4g; see also Supplementary Fig. 6). These findings all suggest that UDP/$P2Y_6$-receptor-mediated signals are important for microglial phagocytosis even *in vivo*.

A recent review described that dying cells use both 'find-me' and 'eat-me' signals for phagocyte attraction and recognition[26]. Nucleotides could be both 'find-me' and 'eat-me' signals. The intracellular ATP concentration is estimated to be high (more than 5 mM) and the UTP concentration is reported to be one-third that of ATP[23]. Cells release ATP, and here we showed that KA caused an increase in extracellular UTP or UDP. Microglia might therefore be attracted by ATP or ADP[5,6] and subsequently recognize UDP, leading to the removal of the dying cells or their debris. It is interesting that ATP/ADP is not able to efficiently activate $P2Y_6$ receptors; neither can UDP act on $P2Y_{12/13}$ receptors. Thus, even if these nucleotides were leaked or released simultaneously, adenine and uridine nucleotides would regulate microglial motilities, namely chemotaxis and phagocytosis, in a mutually exclusive but coordinated fashion.

So far we have not shown quantitative data indicating that individual microglia upregulate the expression of $P2Y_6$ receptors. A significant, but not drastic, increase in $P2Y_6$ receptor protein in the hippocampus was observed after injection of KA (Fig. 3A, B). ISH data show that expression of mRNA coding for $P2Y_6$ receptors in microglia was very low in naive animals but became obvious in an increased number of microglia after KA injection (Fig. 3E), suggesting that the increase in $P2Y_6$ receptor protein is not due simply to an increased number of microglia but is upregulated in individual

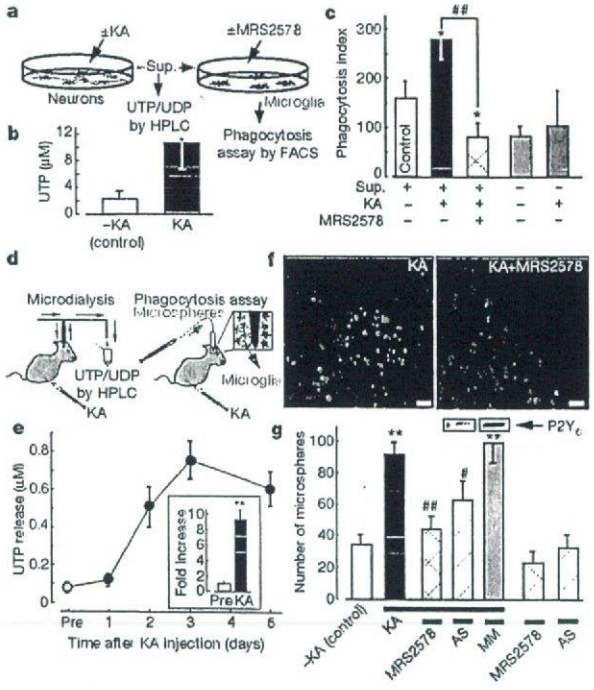

Figure 4 | KA-evoked increases in extracellular uridine nucleotides and $P2Y_6$-receptor-mediated microglial phagocytosis *in vitro* and *in vivo*. **a**, Schematic diagram of the experiments *in vitro*. Sup., supernatant. **b**, Summary of the UTP concentration in the KA-treated and control supernatants. Data show means and s.e.m. for at least five independent experiments (asterisk, $P < 0.05$ compared with control). **c**, Effects of the KA-treated and control supernatant on microglial uptake of fluorescent latex beads. Data show means and s.e.m. for at least four independent experiments (asterisk, $P < 0.05$ compared with control; hash sign, $P < 0.05$ compared with KA-treated supernatant). **d**, Schematic diagram of the experiments *in vivo*. KA was applied intraperitoneally at 10 mg kg^{-1}. **e**, Time course of changes in $[UTP]_o$ in baseline dialysates (before treatment with KA (Pre), and 1, 2, 3 and 5 days afterwards). Inset, fold increase at day 3 (compared with before treatment). **f**, Typical pictures of fluorescent microspheres (green) attached or taken up by microglia (red, anti-Iba1) in the KA-treated (left) and KA + MRS2578-treated (right) hippocampal CA3 regions. Scale bar, 20 μm. **g**, Quantitative analysis of phagocytosis *in vivo* (details are provided in Supplementary Methods). Changes in $P2Y_6$ receptor protein by $P2Y_6$ AS or MM are shown at the top of corresponding columns. Values are means and s.e.m. (asterisk, $P < 0.01$ compared with control (−KA); hash sign, $P < 0.05$; two hash signs, $P < 0.01$ compared with KA-treated group). Statistical analyses were performed by ANOVA with Scheffe's multiple comparison. At least three sections containing the injection sites were analysed per animal, and at least three animals were used in each group for analysis.

microglia. We also emphasize that even if the extent of $P2Y_6$ receptor upregulation is not drastic, an increase in extracellular UDP, a ligand for $P2Y_6$ receptor, is markedly increased after treatment with KA (detected as UTP, almost 10-fold; Fig. 4e) and therefore that the UDP/$P2Y_6$ receptor system would be sufficiently activated to cause microglial phagocytosis after treatment with KA. In comparison with the extensive knowledge of the molecular events involved in the regulation of apoptosis or necrosis, relatively little is known about the processes responsible for the clearance of dead cells and the degradation of waste materials. Considering the present findings that injured neurons leak diffusible UTP/UDP and cause the upregulation of $P2Y_6$ receptors in microglia, the UDP/$P2Y_6$ receptor system might function as a critical device covering the phagocytosis of both apoptotic and necrotic cells if they release or leak UDP by sensing diffusible UDP signals.

Thus we have shown that microglia express $P2Y_6$ receptors that function as a sensor of phagocytosis. The $P2Y_6$ receptor agonist UDP is released (as UTP) when neurons are damaged by KA. Thus, the activation of $P2Y_6$ receptors by UDP would be a key event in initiating the clearance of dying cells or debris in the central nervous system.

METHODS

Detailed methods are provided in Supplementary Information.

Microglia culture. The protocol was reviewed and approved by the Committee for Institutional Laboratory Animal Care of the National Institute of Health Sciences. Rat primary cultured microglia were prepared in accordance with the method described previously[27].

Phagocytosis assay *in vitro* and *in vivo*. *In vitro* microglial phagocytosis was assessed by either FACScan analysis or imaging analysis with fluorescently labelled microspheres. For the *in vivo* phagocytosis assay, fluorescently labelled microspheres were injected into the hippocampal CA3 region after injection of KA, and then the number of fluorescent microspheres associated with microglia was analysed by confocal microscopy (LSM 5 Pascal; Carl Zeiss).

Microdialysis. A microdialysis probe (A-1 type probe; Eicom) was inserted into the hippocampal CA3 region by means of a guide cannula, and was perfused continuously at a flow rate of 3.0 μl min^{-1} (collected for 60 min) supplemented with the ectonuclease inhibitor ARL67156 (20 μM) (Sigma).

Quantification of UTP by HPLC. The concentration of nucleotides in the supernatant of the hippocampal cultures was analysed with an HPLC system (Jasco) combined with a C_{18} column (4.6 × 250 mm, Shodex) as described[28], with minor modifications.

Data analysis and statistics. All results are expressed as means ± s.e.m. A statistical analysis was performed with Student's *t*-test or analysis of variance, followed by Scheffe's multiple comparison test. Differences were considered to be significant at $P < 0.05$.

Received 23 December 2006; accepted 23 February 2007.
Published online 4 April 2007.

1. Guthrie, P. B. *et al.* ATP released from astrocytes mediates glial calcium waves. *J. Neurosci.* 19, 520–528 (1999).
2. Koizumi, S., Fujishita, K., Tsuda, M., Shigemoto-Mogami, Y. & Inoue, K. Dynamic inhibition of excitatory synaptic transmission by astrocyte-derived ATP in hippocampal cultures. *Proc. Natl Acad. Sci. USA* 100, 11023–11028 (2003).
3. Nimmerjahn, A., Kirchhoff, F. & Helmchen, F. Resting microglial cells are highly dynamic surveillants of brain parenchyma *in vivo*. *Science* 308, 1314–1318 (2005).
4. Davalos, D. *et al.* ATP mediates rapid microglial response to local brain injury *in vivo*. *Nature Neurosci.* 8, 752–758 (2005).
5. Honda, S. *et al.* Extracellular ATP or ADP induce chemotaxis of cultured microglia through $G_{i/o}$-coupled P2Y receptors. *J. Neurosci.* 21, 1975–1982 (2001).
6. Nasu-Tada, K., Koizumi, S. & Inoue, K. Involvement of β1 integrin in microglial chemotaxis and proliferation on fibronectin: different regulations by ADP through PKA. *Glia* 52, 98–107 (2005).
7. Ferrari, D. *et al.* P2Z purinoreceptor ligation induces activation of caspases with distinct roles in apoptotic and necrotic alterations of cell death. *FEBS Lett.* 447, 71–75 (1999).
8. Suzuki, T. *et al.* Production and release of neuroprotective tumor necrosis factor by P2X7 receptor-activated microglia. *J. Neurosci.* 24, 1–7 (2004).
9. Tsuda, M. *et al.* P2X4 receptors induced in spinal microglia gate tactile allodynia after nerve injury. *Nature* 424, 778–783 (2003).
10. Chang, K., Hanaoka, K., Kumada, M. & Takuwa, Y. Molecular cloning and functional analysis of a novel P2 nucleotide receptor. *J. Biol. Chem.* 270, 26152–26158 (1995).
11. Communi, D., Parmentier, M. & Boeynaems, J. M. Cloning, functional expression and tissue distribution of the human P2Y6 receptor. *Biochem. Biophys. Res. Commun.* 222, 303–308 (1996).
12. Mamedova, L. K., Joshi, B. V., Gao, Z. G., von Kugelgen, I. & Jacobson, K. A. Diisothiocyanate derivatives as potent, insurmountable antagonists of P2Y6 nucleotide receptors. *Biochem. Pharmacol.* 67, 1763–1770 (2004).
13. Greenberg, S. Signal transduction of phagocytosis. *Trends Cell Biol.* 5, 93–99 (1995).
14. Mitchison, T. J. & Cramer, L. P. Actin-based cell motility and cell locomotion. *Cell* 84, 371–379 (1996).
15. Lauffenburger, D. A. & Horwitz, A. F. Cell migration: a physically integrated molecular process. *Cell* 84, 359–369 (1996).
16. Ohsawa, K., Imai, Y., Kanazawa, H., Sasaki, Y. & Kohsaka, S. Involvement of Iba1 in membrane ruffling and phagocytosis of macrophages/microglia. *J. Cell Sci.* 113, 3073–3084 (2000).
17. Kreutzberg, G. W. Microglia: a sensor for pathological events in the CNS. *Trends Neurosci.* 19, 312–318 (1996).
18. Nicholas, R. A. *et al.* Pharmacological and second messenger signalling selectivities of cloned P2Y receptors. *J. Auton. Pharmacol.* 16, 319–323 (1996).
19. Mellor, E. A., Maekawa, A., Austen, K. F. & Boyce, J. A. Cysteinyl leukotriene receptor 1 is also a pyrimidinergic receptor and is expressed by human mast cells. *Proc. Natl Acad. Sci. USA* 98, 7964–7969 (2001).
20. Lauber, K. *et al.* Apoptotic cells induce migration of phagocytes via caspase-3-mediated release of a lipid attraction signal. *Cell* 113, 717–730 (2003).
21. Bard, F. *et al.* Peripherally administered antibodies against amyloid β-peptide enter the central nervous system and reduce pathology in a mouse model of Alzheimer disease. *Nature Med.* 6, 916–919 (2000).
22. Sperk, G. *et al.* Kainic acid induced seizures: neurochemical and histopathological changes. *Neuroscience* 10, 1301–1315 (1983).
23. Lazarowski, E. R., Homolya, L., Boucher, R. C. & Harden, T. K. Direct demonstration of mechanically induced release of cellular UTP and its implication for uridine nucleotide receptor activation. *J. Biol. Chem.* 272, 24348–24354 (1997).
24. Lazarowski, E. R., Shea, D. A., Boucher, R. C. & Harden, T. K. Release of cellular UDP-glucose as a potential extracellular signaling molecule. *Mol. Pharmacol.* 63, 1190–1197 (2003).
25. Erlinge, D. *et al.* Uridine triphosphate (UTP) is released during cardiac ischemia. *Int. J. Cardiol.* 100, 427–433 (2005).
26. Ravichandran, K. S. 'Recruitment signals' from apoptotic cells: invitation to a quiet meal. *Cell* 113, 817–820 (2003).
27. Nakajima, K. *et al.* Identification of elastase as a secretory protease from cultured rat microglia. *J. Neurochem.* 58, 1401–1408 (1992).
28. Lazarowski, E. R., Boucher, R. C. & Harden, T. K. Constitutive release of ATP and evidence for major contribution of ecto-nucleotide pyrophosphatase and nucleoside diphosphokinase to extracellular nucleotide concentrations. *J. Biol. Chem.* 275, 31061–31068 (2000).

Supplementary Information is linked to the online version of the paper at www.nature.com/nature.

Acknowledgements We thank T. Shimizu and Dr. S. Ishii for providing CysLT1 receptor-expressed Chinese hamster ovary cells; K. Sakemi for technical assistance; Y. Sasaki for helpful suggestions; K. Suzuki and R. Adachi for allowing us to use the Pascal confocal microscope system; and T. Nishimaki-Mogami, Y. Ohno and T. Nagao for continuous encouragement. This study was supported in part by a grant from The National Institute of Biomedical Innovation, a grant from Uehara Memorial Foundation, a Grant-in-Aid for Scientific Research on Priority Areas, for Creative Scientific Research, Scientific Research (A and B), and for Young Scientists (A) from the Ministry of Education, Science, Sports and Culture of Japan.

Author Contributions S.K. designed most experiments, performed Ca^{2+} imaging and *in vivo* experiments and wrote the paper. Y.S.M. conducted major parts of the experiments. K.N.T. and Y.S. carried out the FACS assay and the HPLC analysis, respectively. K.O. and S.K. performed the chemotaxis analysis. B.V.J. and K.A.J. made the $P2Y_6$ receptor antagonist MRS2578. M.T. analysed the data. K.I. analysed the data and coordinated the project. K.I. also designed the project. All authors discussed the results and commented on the manuscript.

Author Information Reprints and permissions information is available at www.nature.com/reprints. The authors declare no competing financial interests. Correspondence and requests for materials should be addressed to K.I. (inouei@phar.kyushu-u.ac.jp).

GLIA 54:606–618 (2006)

Extracellular ATP Counteracts the ERK1/2-Mediated Death-Promoting Signaling Cascades in Astrocytes

YOUICHI SHINOZAKI,[1] SCHUICHI KOIZUMI,[1] YASUO OHNO,[2] TAKU NAGAO,[2] AND KAZUHIDE INOUE[3]*
[1]*Division of Pharmacology, National Institute of Health Sciences, Setagaya, Tokyo 158-8501, Japan*
[2]*National Institute of Health Sciences, Setagaya, Tokyo 158-8501, Japan*
[3]*Department of Molecular and System Pharmacology, Graduate School of Pharmaceutical Sciences, Kyushu University, Higashi-ku, Fukuoka 812-8582, Japan*

KEY WORDS
purinergic receptor; oxidative stress; ERK1/2; src family; protein tyrosine phosphatase

ABSTRACT
Oxidative stress is the main cause of neuronal death in pathological conditions. Hydrogen peroxide (H_2O_2), one of the reactive oxygen species, activates many intracellular signaling cascades including src family and mitogen-activated protein kinases (MAPKs), some of which are critically involved in the induction of cellular damage. We previously showed that H_2O_2-induced cell death in astrocytes and adenosine 5′-triphosphate (ATP), acting on $P2Y_1$ receptors, had a protective effect. Here, we examined the H_2O_2-induced changes in intracellular signaling cascades that promote cell death in astrocytes, showing the molecular mechanisms by which the activation of $P2Y_1$ receptors counteracts such signals. Although H_2O_2 activated three MAPKs including ERK1/2, p38, and JNK, only the activation of ERK1/2 participated in the H_2O_2-evoked cell death. H_2O_2 induced a sustained activation of ERK1/2 mainly in the nucleus region, which was well in accordance with the H_2O_2-induced cell death. H_2O_2 also activated the src tyrosine kinase family, which was an upstream signal for ERK1/2. Activation of $P2Y_1$ receptors by 2methylthio-ADP (2MeSADP) inhibited the H_2O_2-evoked activation of src tyrosine kinase, resulting in the inhibition of the phosphorylated-ERK1/2 accumulation in the nucleus. 2MeSADP enhanced the gene expression and activity of protein tyrosine phosphatase (PTP), which was responsible for the inhibition of src tyrosine kinase. Thioredoxin reductase, another cytoprotective gene we previously showed to be upregulated by 2MeSADP, also controlled the activity of PTP. Taken together, ATP, acting on $P2Y_1$ receptors, upregulates the PTP expression and its activity, which counteracts the H_2O_2-promoted death signaling cascades including ERK1/2 and its upstream signal src tyrosine kinase in astrocytes.

INTRODUCTION

Adenosine 5′-triphosphate (ATP) is an important signaling molecule that mediates gliotransmission and also glia-to-neuron communication in the CNS (Fields and Stevens-Graham, 2002; Hansson and Ronnback, 2003; Inoue, 2002). The $P2Y_1$ receptor has a central role in the ATP-mediated gliotransmission in astrocytes (Fam et al., 2000) and we previously demonstrated that ATP, acting on $P2Y_1$ receptors, protected astrocytes against oxidative stress, indicating the physiological importance of ATP-mediated gliotransmission in astrocytes (Shinozaki et al., 2005). However, details concerning the molecular mechanism(s) by which $P2Y_1$ receptor activation results in such protection are still lacking.

Hydrogen peroxide (H_2O_2), one of the reactive oxygen species (ROS), activates various intracellular signaling cascades including mitogen-activated protein kinases (MAPKs) (Fialkow et al., 1994; Konishi et al., 1999; Ushio-Fukai et al., 1999). The MAPK family includes extracellular signal-regulated kinase 1 and 2 (ERK1/2), p38 kinase, and c-Jun NH_2-terminal kinase (JNK). The latter two members are well known to be stress-responding MAPKs, which are activated by lipopolysaccharide, cytokines, and oxidative stress such as by H_2O_2 and induce cell death (Oppenheim, 1991). ERK1/2 is constitutively expressed in various regions including the CNS (Boulton et al., 1991). ERK1/2 is activated by various neurotransmitters, hormones and growth factors in physiological conditions, controls the transcription factor activity and induces various physiological responses, such as cell proliferation or differentiation (Boulton et al., 1991; Marshall, 1995; Segal and Greenberg, 1996). However, ERK1/2 is also activated by various types of stress such as oxidative stress or shear stress, and appears to control the survival of cells (Guyton et al., 1996; Takahashi and Berk, 1996; Wang et al., 1998; Xia et al., 1995). Concerning neuronal cells, recent reports have shown that activation of ERK1/2 even promotes cell death both in vivo and in vitro (Murray et al., 1998; Namura et al., 2001; Stanciu and DeFranco, 2002; Subramaniam et al., 2004). Thus, although ERK1/2 is an essential intracellular signaling molecule that mediates various physiological functions, it may also mediate the death of cells. The intensity of ERK1/2 activation and spatial and temporal differences in its activation would greatly affect physiological or pathophysiological events in cells.

The src family, a well-known protein tyrosine kinase (PTK), regulates a variety of cellular functions such as cell

Grant sponsor: The National Institute of Biomedical Innovation, MF-16 grant; Grant sponsor: Uehara Memorial Foundation; Grant sponsor: Scientific Research (B) for Young Scientists (A) and on Priority Areas (A), Ministry of Education, Science, Sports and Culture, Japan.

*Correspondence to: Kazuhide Inoue, Department of Molecular and System Pharmacology, Graduate School of Pharmaceutical Sciences, Kyushu University, Maidashi 3-1-1, Higashi-ku, Fukuoka 812-8582, Japan.
E-mail: inoue@phar.kyushu-u.ac.jp

Received 1 December 2005; Revised 21 July 2006; Accepted 25 July 2006

DOI 10.1002/glia.20408

Published online 30 August 2006 in Wiley InterScience (www.interscience.wiley.com).

growth, proliferation, and differentiation. The src family is abundantly expressed in the CNS (Brugge et al., 1985; Sugrue et al., 1990), and is also involved in brain injury induced by oxidative stress. In fact, H_2O_2 or ischemia/reperfusion injury activates the src family in the hippocampus (Guo et al., 2003; Ohtsuki et al., 1996). Activation of the src family is prevented by protein tyrosine phosphatase (PTP). PTP is related to various events in the CNS such as inhibition of the NMDA receptor activation in neurons(Yu and Salter, 1999) and of microglial TNFa and nitric oxide generation by amyloid β (Tan et al., 2000). In addition, PTP upregulation is observed in kainic acid-treated (Boschert et al., 1997) and ischemia-injured neurons (Takano et al., 1996). Thus, the activity and expression of PTP is also important for the regulation of pathophysiological cellular functions as well as the regulation of src tyrosine kinase.

On the basis of these findings, we hypothesized that MAPKs and src family are key molecules for promoting the H_2O_2-evoked cell death in astrocytes and that ATP acting on $P2Y_1$ receptors may counteract these cell death-promoting signaling cascades.

In the present study, we demonstrate that activation of both src tyrosine kinase and the subsequent ERK1/2 are key events in the H_2O_2-evoked cell death in astrocytes. We also demonstrate that ATP/$P2Y_1$ receptor activation interferes with the H_2O_2-evoked src family—ERK1/2 cascades by increasing the expression and activity of PTP, thereby leading to protection against H_2O_2-induced cell death in astrocytes.

MATERIALS AND METHODS

Chemicals

Adenosine 5′-triphosphate (ATP), adenosine, 2-methylthio adenosine diphosphate (2MeSADP), bovine serum albumin (BSA), propidium iodide (PI), sodium orthovanadate (Na_3VO_4), MRS2179, and *N*-acetyl cystein were purchased from Sigma Chemical (St Louis, MO). The sources of other chemicals are shown in parentheses as follows; hydrogen peroxide (H_2O_2) (Wako Pure Chemicals, Osaka, Japan), 3-(4,5-dimethylthiazol-2-y1)-2,5-diphenyltetrazolium bromide (MTT) assay kit (CHEMICON International, Temecula, CA), PD98059, U0126, SB203580, SP600125, and PP3 (Calbiochem Biosciences, San Diego), PP1 and PP2 (Biosource, CA), auranofin (Alexis biochemicals, Lausen, Switzerland).

Abbreviations

ATP	adenosine 5′-triphosphate
2MeSADP	2-methylthio-adenosine 5′-diphosphate
ERK1/2	extracellular signal-regulated kinase 1 and 2
H_2O_2	hydrogen peroxide
JNK	c-Jun NH_2-terminal kinase
MAPK	mitogen-activated protein kinase
MAPKP	MAPK phosphatase
MEK1/2	MAPK kinase 1 and 2
Na_3VO_4	sodium orthovanadate
PI	propidium iodide
PTK	protein tyrosine kinase
PTP	protein tyrosine phosphatase
P-Tyr	phosphorylated tyrosine
ROS	reactive oxygen species
TrxR	thioredoxin reductase

Antibodies

Polyclonal antibodies against total ERK1/2, phosphorylated ERK1/2, phosphorylated p38, and phosphorylated JNK were purchased from Cell Signaling Technology (Beverly, MA). The monoclonal antibody against phosphorylated tyrosine was purchased from Sigma Chemical (St Louis, MO).

Cells and Cell Culture

Astrocytes were prepared from neonatal rat forebrain. The cells were cultured as previously reported (Shinozaki et al., 2005). For the cell viability assay, cells were seeded on 96-well plates (NUNC, Roskilde, Denmark) at a density of 1.25×10^4 cells/well.

Cell Viability Assay

For the cell viability assay, we used an MTT assay as previously reported (Shinozaki et al., 2005). A 1/10 volume of MTT solution (5 mg/mL in PBS) was added and incubated for 4 h under 10% CO_2/90% air at 37°C. Then, an equal volume of isopropanol (with 0.04 N HCl) was added to the cells. The absorbance was measured on an ELISA plate reader (ASYS Hitech, Eugendorf, Austria) with a test and reference wavelength of 570 and 630 nm, respectively.

Western Blotting

Astrocytes were prepared as described above. After H_2O_2-stimulation, cells were lysed and the lysates were resolved with 10% SDS-PAGE gels and transferred to PVDF membranes. The membranes were blocked for 1 h in Tris-buffered saline containing 0.1% Tween-20 (TBS/T) and 5% non-fat dry milk at room temperature. Then the membranes were incubated with primary antibody dilution buffer (1:1000 dilution into TBS/T containing 5% BSA) overnight at 4°C. After three washes with TBS/T, the membranes were incubated with horseradish peroxidase-conjugated anti-rabbit antibody (1:2000 dilution into TBS/T containing 5% non-fat dry milk) for 1 h at room temperature. The membranes were washed with TBS/T three times, and the proteins were visualized by chemiluminescence. The antibodies for anti-phospho-proteins used in the present study (anti-P-ERK1/2, P-p38, and P-JNK or P-Tyr antibodies) specifically detected only the activated and phosphorylated form of the proteins. To detect total ERK1/2, the aliquot of the same sample was resolved with 10% SDS-PAGE gels, transferred to PVDF membranes in the same conditions and exposed to anti-total ERK1/2 antibody.

Quantification of the Intensity of P-ERK1/2 Bands

To quantify the intensity of P-ERK1/2 bands, we used Image J (http://rsb.info.nih.gov/ij/). P-ERK1/2 bands were selected by rectangular selection. Then, we selected *Analyze-Gels-Select First Lane* from the menu bar. The

area corresponding to each band was measured using *Wand (tracing) tool* from the tool bar.

Immunocytochemistry

After each treatment, the cells were fixed for 30 min at room temperature in 3.7% paraformaldehyde. The fixed cells were permeabilized with PBS containing 0.1% Triton X-100 for 5 min at room temperature and then incubated with the polyclonal anti-ERK1/2 and anti-phospho-ERK1/2 antibodies for 24 h at 4°C. After washing, the cells were incubated with the appropriate secondary antibodies conjugated to Alexa 488 or 546, washed again, and mounted on glass coverslips (Matsunami Glass, Osaka, Japan). Astrocytes for immunocytochemistry were selected randomly. Images were collected in an MRC-1024 laser-scanning microscope (Bio-Rad) with 20× objective lenses. For the comparison of double-stained patterns, images were processed using Photoshop 5 (Adobe System, Mountain View, CA).

Tyrosine Phosphatase Assay

The tyrosine phosphatase activity was measured using a universal tyrosine phosphatase kit (Takara, Shiga, Japan). The measurement was done according to the manufacturer's instructions. Cells were lysed by lysis buffer and transferred into 96-well ELISA plates at a volume of 50 μL/well followed by incubation for 45 min at 37°C. After four times washing with tween-PBS (PBS containing 0.05% tween20), blocking buffer was added to the wells at a volume of 100 μL/well followed by 30 min incubation at 37°C. Then, the blocking buffer was discarded and coloring substrates were added to the wells (100 μL/well). After a 15 min incubation at room temperature, 1 N sulfuric acid was added to the wells (100 μL/well) to stop the reaction. The absorbance was measured by a plate reader (ASYS Hitech, Eugendorf, Austria) at a test wavelength of 450 nm.

Quantitative RT-PCR of PTP Genes

RT-PCR amplifications were performed using Taqman One-step RT-PCR Master Mix Reagents and 200 nM PTP specific primers as previously reported (Shinozaki et al., 2005). Using the computer software Primer Express (Applied Biosystems), clone-specific primers were designed to recognized rat PTP genes, i.e., rat PTP4a1 (Taqman probe, 5′-acacaatccaaccaatgcgacgttaaacaa-3′; forward, 5′-tgctcctgtggaagtcacataca-3′; reverse, 5′-gtcgtaagttgcttcgcatactctta-3′) and rat PTPro (Taqman probe, 5′-ccgctatacaaacatcctgccgtacgactt-3′; forward, 5′-ttccgctgaaccgatgtaaaa-3′; reverse, 5′-tgaggtgagttgtagccaggaata-3′). RT-PCR was performed by 30 min reverse transcription at 48°C, 10 min Amplitaq Gold activation at 95°C, then 15-s denaturation at 95°C, 1 min annealing and elongation at 60°C for 40 cycle in a PRISM7700 (Applied Biosystems). Each experiment was performed in triplicate.

RESULTS

MEK1/2 Inhibitors Protect Astrocytes Against H_2O_2-Evoked Cell Death

Figure 1A shows the effect of H_2O_2 on the activation of MAPKs in astrocytes. Western blotting analysis revealed that stimulation of astrocytes with 250 μM H_2O_2 for 2 h resulted in the activation of three MAPKs, i.e., ERK1/2, p38, and JNK (Fig. 1A). We then tested pharmacologically whether the activation of these MAPKs is involved in the H_2O_2-evoked cell death in astrocytes. The H_2O_2-induced decrease in the cell viability of the astrocytes obtained from the MTT assay was always accompanied by the activation of caspase-3, DNA damage, and nucleus condensation (data not shown). Thus, we defined the decrease in cell viability as cell death in astrocytes in the following experiments. MAPK kinase 1/2 (MEK1/2) activates ERK1/2. The MEK1/2 inhibitors PD98059 (10 μM) (Alessi et al., 1995) and U0126 (20 μM) (Favata et al., 1998) strongly inhibited the H_2O_2-evoked cell death (Fig. 1B). The inhibitory

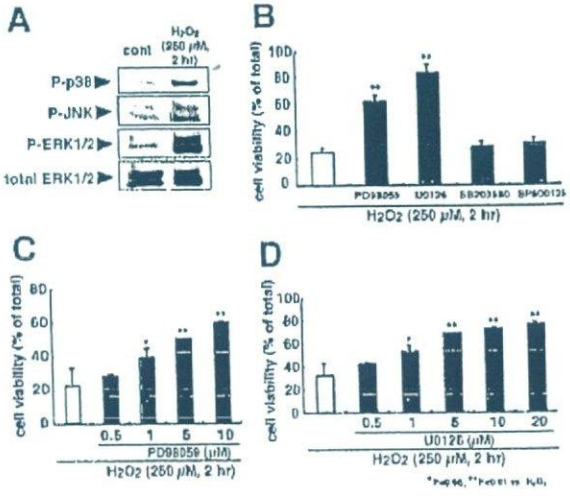

Fig. 1. The effect of MAPK inhibitors on the H_2O_2-evoked cell death of astrocytes. A: The effect of H_2O_2 on MAPK activation in astrocytes. H_2O_2 (250 μM, 2 h) activated p38, JNK, and ERK1/2. B: The effect of MAPK inhibitors on H_2O_2-evoked cell death. The MEK1/2 inhibitors PD98059 (10 μM) and U0126 (20 μM) strongly inhibited the H_2O_2-evoked cell death. Neither the JNK inhibitor SP600125 (20 μM) nor the p38 inhibitor SB203580 (20 μM) affected the H_2O_2-evoked cell death. C: The concentration-dependent effect of PD98059 against H_2O_2-evoked cell death. The protective effect of PD98059 was dose-dependent in a concentration range from 0.5 to 10 μM. D: The concentration-dependent effect of U0126 against H_2O_2-evoked cell death. The protective effect of U0126 was dose-dependent in a concentration range from 0.5 to 20 μM. Neither inhibitor alone affected the cell viability of the astrocytes. Inhibitors added to the cells 1 h before H_2O_2 treatment. Asterisks show significant difference from the response evoked by H_2O_2 (*$P < 0.05$, **$P < 0.01$ vs. H_2O_2 alone, Student's *t*-test). Results were expressed as means ± SEM of triplicate measurements ($n = 3$).

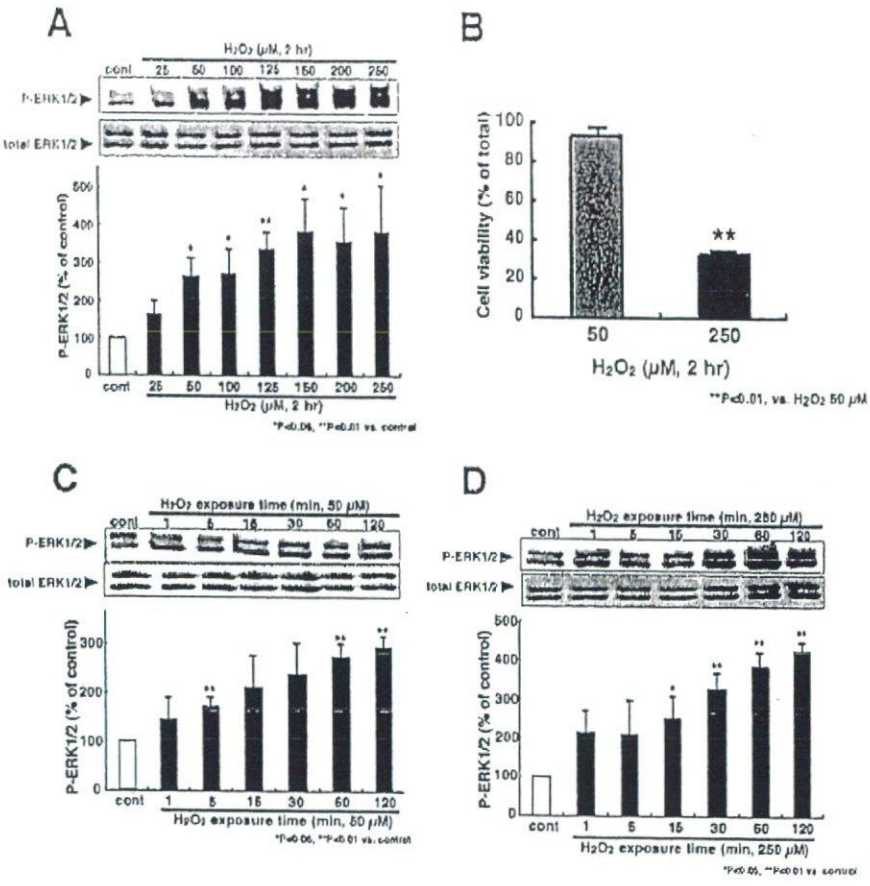

Fig. 2. The concentration-dependency and time course of the H_2O_2-evoked ERK1/2 activation in the astrocytes. A: The concentration-dependency of the H_2O_2-evoked ERK1/2 activation. H_2O_2 activated ERK1/2 in a concentration-dependent fashion at the whole cell level (0–250 μM, 2 h). H_2O_2 did not affect the amount of total ERK1/2. Asterisks show significant difference from control ($^*P < 0.05$, $^{**}P < 0.01$ vs. control, Student's *t*-test). B: The degree of the decrease of the cell viability of H_2O_2-treated astrocytes markedly decreased the cell viability in the astrocytes 250 μM but not at 50 μM H_2O_2. Asterisks show significant difference from the response evoked by H_2O_2 ($^{**}P < 0.01$ vs. 50 μM H_2O_2, Student's *t*-test). C and D: A temporal analysis of the H_2O_2-evoked ERK1/2 activation in the astrocytes. At the whole cell level, ERK1/2 was activated by H_2O_2 treatment time dependently (0–120 min) despite the concentration of H_2O_2 (50 and 250 μM). H_2O_2 did not affect the total ERK1/2. Asterisks show significant difference from control ($^*P < 0.05$, $^{**}P < 0.01$ vs. control, Student's *t*-test). Results were expressed as means ± SEM of triplicate measurements ($n = 3$).

effects by PD98059 and U0126 were dose-dependent in a concentration-range from 0.5 to 10 μM (Fig. 1C) and 0.5 to 20 μM (Fig. 1D), respectively. In contrast, neither the p38 inhibitor SB203580 (Alessandrini et al., 1999; McLaughlin et al., 1996) nor the JNK inhibitor SP600125 (20 μM) (Bennett et al., 2001) had any effect on the H_2O_2-evoked cell death.

The Concentration-Dependency and Time Course of H_2O_2-Evoked ERK1/2 Activation

Among the H_2O_2-activated MAPKs tested, only ERK1/2 was involved in the H_2O_2-evoked cell death (Fig. 1B). H_2O_2 activated ERK1/2 in a concentration- and exposure time-dependent fashion at the whole cell level (Figs. 2A,C,D). Although a lower H_2O_2 concentration (50 μM) activated ERK1/2, H_2O_2 at this concentration did not cause cell death (Fig. 2B). At a higher concentration, H_2O_2 (250 μM) evoked ERK1/2 phosphorylation and cell death in astrocytes (Figs. 2A,B). The phosphorylation of ERK1/2 evoked by 250 μM H_2O_2 was stronger than that evoked by 50 μM H_2O_2. H_2O_2 at either concentration did not affect the total ERK1/2 at the whole cell level.

The Temporal and Spatial Aspect of P-ERK1/2 Induced by H_2O_2

We investigated the temporal and spatial distribution of P-ERK1/2 using immunocytochemical techniques. H_2O_2-evoked ERK1/2 activation was observed in GFAP-positive astrocytes (data not shown). It was reported that ERK1/2 is translocated into the nucleus from the cytoplasm when it is activated (Chen et al., 1992; Gonzalez et al., 1993). We thus analyzed the distribution of P-ERK1/2 after H_2O_2 stimulation. When the cells were stimulated with 250 μM H_2O_2 for 2 h, P-ERK1/2 signals were observed in the center part of individual astrocytes and were colocalized with the signals of PI, a DNA binding dye, suggesting that P-ERK1/2 had translocated into the nucleus (Fig. 3A). In contrast, when stimulated with 50 μM H_2O_2 for 2 h which activated ERK1/2 but did not induce cell death, the P-ERK1/2 signals were observed but were not colocalized with the PI signals (Fig. 3A). The total amount of ERK1/2 signals, however, was not affected by H_2O_2 (50 and 250 μM), and they were not colocalized with the PI signals (Fig. 3B). Without H_2O_2 stimulation, the P-ERK1/2 signals were too low (Figs. 2A,D and 3E, cont.) to detect. To quantify the degree of the colocalization of the P-ERK1/2 and PI signals, we

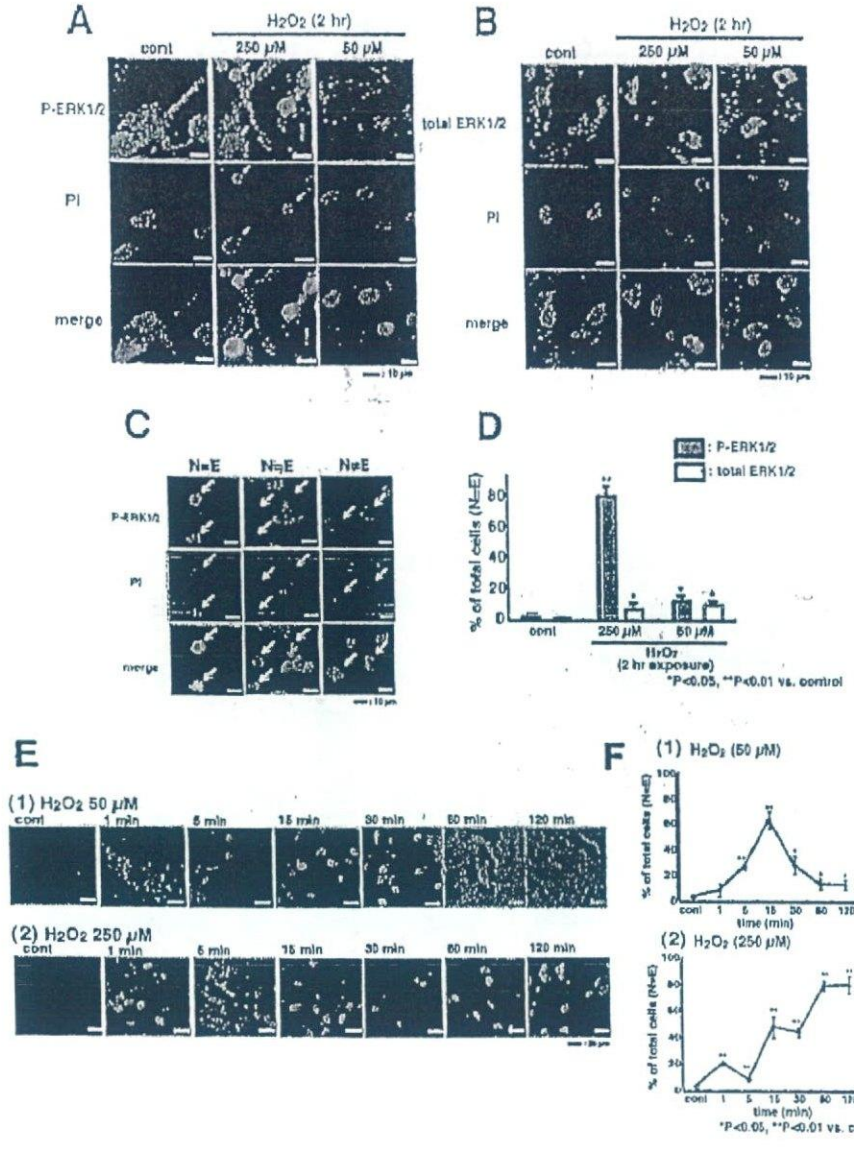

Fig. 3. The effect of H_2O_2 on the intracellular localization of ERK1/2 in astrocytes. A: The effect of H_2O_2 on the intracellular localization of P-ERK1/2. In control, the P-ERK1/2 and PI signals did not colocalize (left). When the cells were treated with 250 μM H_2O_2 (2 h), a large number of P-ERK1/2 and PI signals colocalized (center, arrow). At 50 μM H_2O_2, the P-ERK1/2 and PI signals did not colocalize (right). B: The effect of H_2O_2 on the intracellular localization of total ERK1/2. Total ERK1/2 did not colocalize with the PI signals irrespective of the H_2O_2 treatment (control, 50 and 250 μM). The signals of P-ERK1/2 were enhanced by photoshop to clarify their intracellular localization. C: Classification of the H_2O_2-treated cells into three groups. Astrocytes in which P-ERK1/2 signals were colocalized with PI signals were defined as "N = E" (left), those in which P-ERK1/2 signals were partly colocalized with PI signals were defined as "N ≈ E" (center), and those in which the P-ERK1/2 signals were not colocalized with the PI signals were defined as "N ≠ E" (right). D: Quantification of P-ERK1/2 localization into the nucleus. When cells were stimulated by 250 μM H_2O_2, the colocalization of P-ERK1/2 and PI was observed in most cells but not when they were stimulated by 50 μM H_2O_2. Asterisks show significant difference from control (*$P < 0.05$, **$P < 0.01$ vs. control, Student's t-test). E and F: The temporal analysis of the colocalization of the P-ERK1/2 and PI signals. At 50 μM H_2O_2, N = E cells increased transiently (5–30 min after H_2O_2 stimulation) (E(1), F(1)). At 250 μM H_2O_2, N = E cells increased time-dependently (E(2), F(2)). The DNA binding dye PI was used for identifying the nuclear region. Asterisks show significant difference from control (*$P < 0.05$, **$P < 0.01$ vs. control, Student's t-test). Results were expressed as means ± SEM of triplicate measurements.

classified the cells into three groups, i.e., cells in which P-ERK1/2 signals were colocalized with PI signals (defined as "N = E"), those in which the P-ERK1/2 signals were not colocalized with the PI signals (defined as "N ≠ E"), and P-ERK1/2 signals were partly colocalized with IP signals (defined as "N = E") (Fig. 3C). When stimulated with 50 and 250 μM H_2O_2 for 2 h, the fraction of N = E was 12.7% ± 3.8% (n = 304) and 81.0% ± 6.3% (n = 612), respectively. Without H_2O_2 stimulation, no colocalization of P-ERK1/2 and PI was observed in almost any of the cells (N = E cells, 3% ± 0.2%, n = 346) (Fig. 3D). In contrast to P-ERK1/2, most of the total ERK1/2 signals did not colocalize with PI irrespective of H_2O_2 stimulation(N = E cells, control, 1.3% ± 0.8%, n = 225; 250 μM H_2O_2, 6.5% ± 4.0%, n = 545; 50 μM H_2O_2, 10.7% ± 1.2%, n = 229). Furthermore, we analyzed the time course of the fraction of "N = E" cells after H_2O_2 stimulation. When stimulated with 50 μM H_2O_2, the N = E fraction peaked at 15 min after the stimulation, and the fraction decreased to the prestimulated level after 120 min (N = E cells, 1 min, 7.8% ± 5.4%, n = 201; 5 min, 27.8% ± 2.9%, n = 213; 15 min, 66.6% ± 7.1%, n = 216; 30 min, 29.1% ± 7.4%, n = 226; 60 min, 13.1% ± 4.5%, n = 254; 120 min, 12.7% ± 3.8%, n = 405). In contrast, when stimulated with 250 μM H_2O_2, the N = E fraction gradually increased, reached the maximal level at 60 min, and remained even 120 min after the stimulation (N = E cells, 1 min, 20.7% ± 7%, n = 354; 5 min, 8.1% ± 0.7%, n = 213; 15 min, 48.4% ± 8.3%, n = 220; 30 min, 44.2% ± 3.3%, n = 214; 60 min,

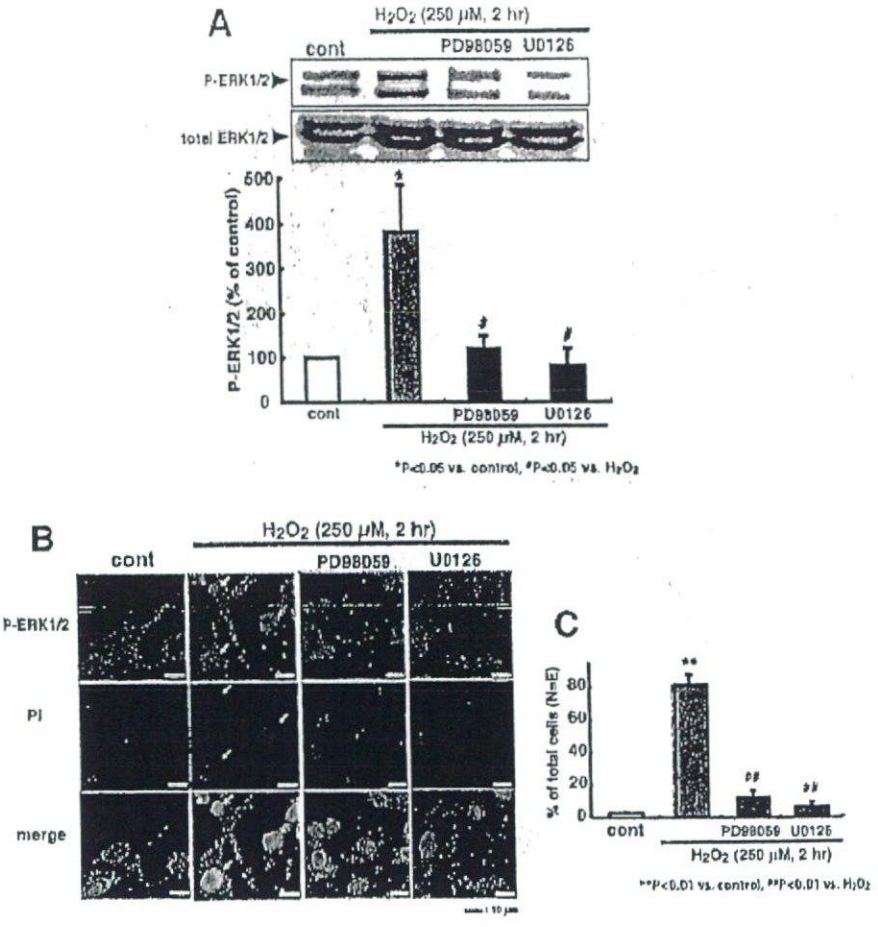

Fig. 4. The effect of MEK1/2 inhibitors on H_2O_2-evoked ERK1/2 activation and P-ERK1/2 translocation. A: The effect of MEK1/2 inhibitors on H_2O_2-evoked ERK1/2 activation. PD98059 (10 μM) and U0126 (20 μM) strongly inhibited the H_2O_2-evoked ERK1/2 activation. Asterisks show significant difference from control (*$P < 0.05$ vs. control, Student's *t*-test). Sharps show significant difference from H_2O_2 (#$P < 0.05$ vs. H_2O_2, Student's *t*-test). Results were expressed as means ± SEM of triplicate measurements ($n = 3$). B and C: The effect of the MEK1/2 inhibitors on the H_2O_2-evoked P-ERK1/2 translocation. PD98059 (10 μM) and U0126 (20 μM) blocked the colocalization of the P-ERK1/2 and PI signals evoked by H_2O_2 (250 μM, 2 h). In the immunocytochemical analysis, the signals of P-ERK1/2 were enhanced by photoshop to clarify their intracellular localization. The DNA binding dye PI was used for identifying the nuclear region. The MEK1/2 inhibitors were applied to the cells 1 h before and during H_2O_2 treatment. Asterisks show significant difference from control (**$P < 0.01$ vs. control, Student's *t*-test). Sharps show significant difference from H_2O_2 (##$P < 0.01$ vs. H_2O_2, Student's *t*-test). Results were expressed as means ± SEM of triplicate measurements.

80.2% ±3.8%, $n = 205$; 120 min, 81%S ± 6.3%, $n = 612$) (Fig. 3F). PD98059 (10 μM) and U0126 (20 μM), at the concentrations that the two inhibitors blocked the H_2O_2-induced cell death (Figs. 1C,D), strongly inhibited the H_2O_2 (250 μM, 2 h)-evoked ERK1/2 activation (Fig. 4A). In addition, these inhibitors prevented the colocalization of P-ERK1/2 and PI, i.e., the H_2O_2-evoked increase in the fraction of N = E was almost abolished (Figs. 4B,C) (N = E cells, PD98059 + H_2O_2, 11.7% ± 3.8%, $n = 524$; U0126 + H_2O_2, 5.9% ± 2.9%, $n = 400$).

ATP Inhibits the H_2O_2-Evoked Activation of ERK1/2 and Its Localization of P-ERK1/2 in the Nucleus

Our previous report by Shinozaki et al., demonstrated that ATP and 2MeSADP inhibited the H_2O_2-induced cell death in astrocytes (Shinozaki et al., 2005). Thus, we examined the effect of ATP and 2MeSADP on the H_2O_2-evoked ERK1/2 activation. In astrocytes pretreated with ATP (100 μM) or 2MeSADP (1 μM) for 24 h, the H_2O_2-induced ERK1/2 activation was markedly inhibited (Fig. 5A). We also analyzed the effect of ATP/2MeSADP on the spatiotemporal behavior of P-ERK1/2 in astrocytes. Immunocytochemical studies showed that pretreatment of the cells with ATP/2MeSADP prevented the H_2O_2-evoked colocalization of P-ERK1/2 and PI signals (Fig. 5B). The fraction of N = E was almost completely inhibited by ATP or 2MeSADP (N = E cells, ATP + H_2O_2, 5.1% ± 3.3%, $n = 340$; 2MeSADP + H_2O_2, 1.1% ± 1.4%, $n = 342$) (Fig. 5C).

ATP itself is known to activate ERK1/2 in some cells including astrocytes (Neary et al., 1999, 2003). Using Western blotting analysis, we found that both ATP (100 μM) and 2MeSADP (1 μM) activated ERK1/2 but the activation was only transient (lasting 1–15 min after stimulation) and returned to the prestimulated level within 120 min [Figs. 6A(i,ii)]. Thus, after the initial phosphorylation of ERK1/2 evoked by ATP/2MeSADP the activation should have returned to the prestimulated level when the astrocytes were stimulated with H_2O_2 24 h after ATP-treatment. Interestingly, when 2MeSADP was pretreated with PD98059 (10 μM) or U0126 (20 μM), the 2MeSADP-induced cytoprotective effects against H_2O_2 disappeared (Fig. 6B). Furthermore, using quantitative RT-PCR, we found that U0126 inhibited the 2MeSADP (1 μM, 2 h)-induced upregula-

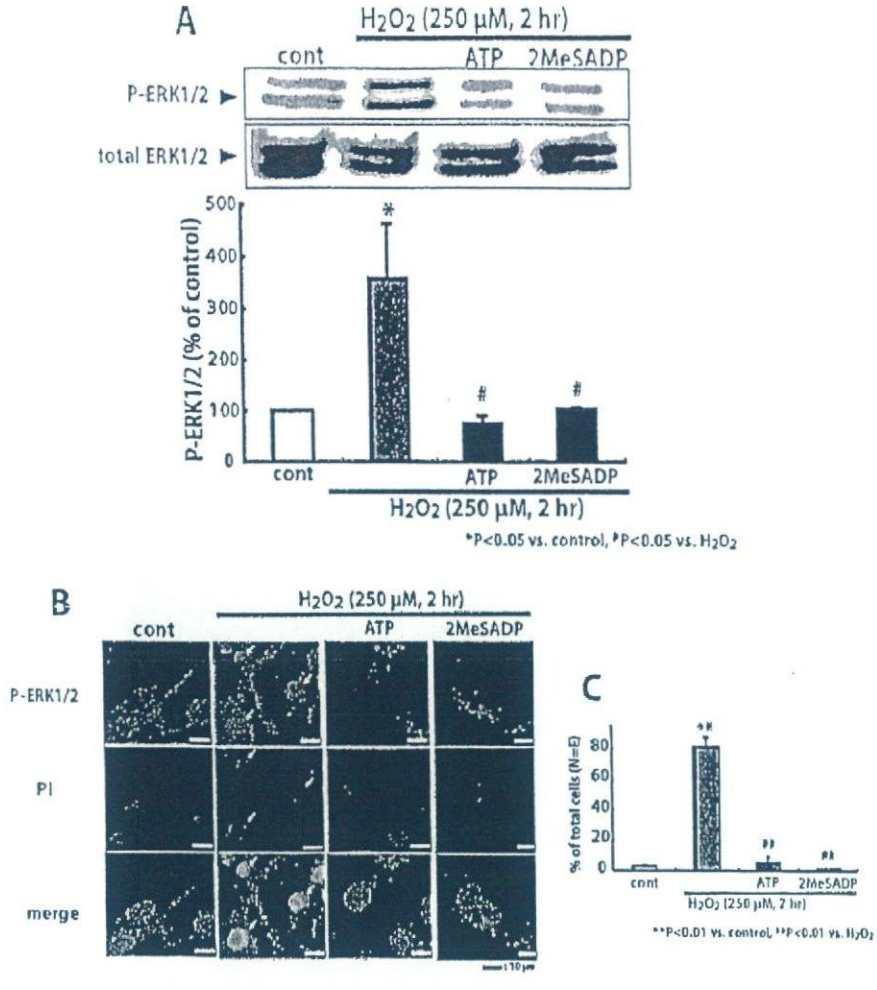

Fig. 5. The effect of ATP and 2MeSADP on H_2O_2-evoked ERK1/2 and P-ERK1/2 translocation. A: The effect of ATP and 2MeSADP on H_2O_2-evoked ERK1/2 activation. ATP (100 μM) and 2MeSADP (1 μM) strongly inhibited the H_2O_2-evoked ERK1/2 activation at the whole cell level. Asterisks show significant difference from control (*$P < 0.05$ vs. control, Student's t-test). Sharps show significant difference from H_2O_2 (#$P < 0.05$ vs. H_2O_2, Student's t-test). Results were expressed as means ± SEM of triplicate measurements ($n = 3$). B and C: The effect of ATP and 2MeSADP on H_2O_2-evoked P-ERK1/2 translocation. ATP (100 μM) and 2MeSADP (1 μM) abolished the colocalization of the P-ERK1/2 and PI signals evoked by H_2O_2 (250 μM, 2 h). In the immunocytochemical analysis, the signals of P-ERK1/2 were enhanced by photoshop to clarify their intracellular localization. The DNA binding dye PI was used for identifying the nuclear region. ATP and 2MeSADP was applied to the cells 24 h before and during H_2O_2 treatment. Asterisks show significant difference from control (**$P < 0.01$ vs. control, Student's t-test). Sharps show significant difference from H_2O_2 (##$P < 0.01$ vs. H_2O_2, Student's t-test). Results were expressed as means ± SEM of triplicate measurements.

tion of thioredoxin reductase (TrxR) (2MeSADP, 232.2% ± 54.4% of control, $P < 0.01$ vs. control; 2MeSADP + U0126, 114.9% ± 9.4% of control, $P < 0.05$ vs. 2MeSADP alone; $n = 3$) and PTPs (PTP4a1: 2MeSADP, 291.1% ± 78.5% of control, $P < 0.05$ vs. control, 2MeSADP + U0126, 102.8% ± 12.2% of control, $P < 0.05$ vs. 2MeSADP alone; $n = 3$; PTPro: 2MeSADP, 608.0% ± 153.8% of control, $P < 0.01$ vs. control; 2MeSADP + U0126, 264.7% ± 47.7% of control, $P < 0.05$ vs. 2MeDADP alone; $n = 3$). U0126 alone did not affect the expression level of TrxR (94.5% ± 30.8% of control; $n = 4$) and PTP genes (PTP4a1, 107.5% ± 21.7% of control; PTPro, 113.6% ± 14.3% of control, $n = 4$). The MEK1/2 inhibitors were added to the cells 1 h before and during 2MeSADP-treatment, and was washed out before the H_2O_2 stimulation. Thus, the phosphorylation of ERK1/2 induced by H_2O_2, represented by the sustained and intense responses seen mainly in the nucleus appeared to cause cell death in the astrocytes, while the ATP-induced transient phosphorylation of ERK1/2 appeared to have a cytoprotective action.

ATP Increases PTP Expression and Its Activity, Leading to Protection Against the H_2O_2-Evoked Cell Death in Astrocytes

We comprehensively studied whether ATP induces the expression of genes that could regulate ERK1/2 activity using a GeneChip microarray. We expected that ATP might upregulate the expression of genes that dephosphorylate ERK1/2 such as MAPK phosphatase (MAPKP), which dephosphorylates ERK1/2, thereby leading to the inactivation of ERK1/2 and the cytoprotective action by ATP. However, no upregulation of any MAPKPs in the GeneChip microarray was observed. Instead, we found the ATP (100 μM, 2 h)-induced upregulation of PTP genes containing PTP4a1 and PTP, receptor type O (PTPro) (Table I).

In the PTP activity assay, both ATP (100 μM, 24 h) and 2MeSADP (1 μM, 24 h) significantly increased the PTP activity (ATP, 148.3% ± 8.8%; 2MeSADP, 168.8% ± 4.8%) (Fig. 7A). Subsequently, we analyzed the effect of the PTP inhibitor sodium orthovanadate (Na_3VO_4)

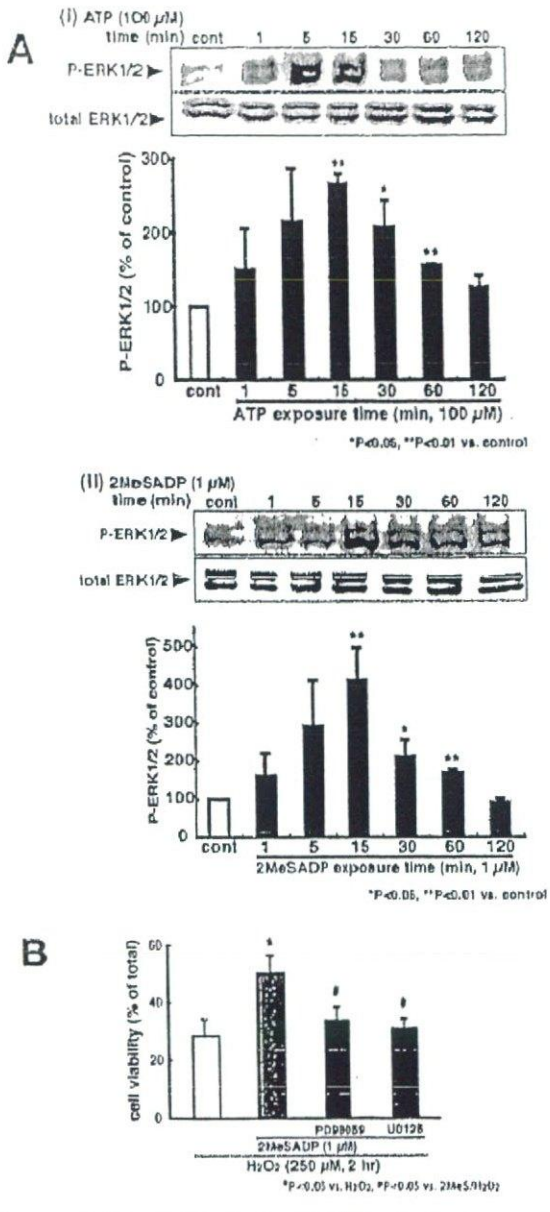

Fig. 6. Analysis of ATP-stimulated ERK1/2 activation in astrocytes. A: The time course of ATP-induced ERK1/2 activation. ATP (100 μM) activated ERK1/2 transiently (1–15 min after stimulation) (i). 2MeSADP (1 μM) also activated ERK1/2 transiently (1–15 min after stimulation) (ii). ATP and 2MeSADP did not affect the total amount of ERK1/2. Asterisks show significant difference from control (*$P < 0.05$, **$P < 0.01$ vs. control, Student's t-test). B: The effect of 2MeSADP-stimulated ERK1/2 on the $P2Y_1$ receptor-mediated cytoprotective effect. The MEK1/2 inhibitors PD98059 (10 μM) and U0126 (20 μM) strongly inhibited the protective effect induced by 2MeSADP (1 μM, 24 h). The MEK1/2 inhibitors were added to the cells 1 h before the 2MeSADP treatment and were washed out before the H_2O_2 treatment. Asterisks show significant difference from the response evoked by H_2O_2 (*$P < 0.05$ vs. 250 μM H_2O_2, Student's t-test). Sharps show significant difference from 2MeSADP/H_2O_2 (#$P < 0.05$ vs. 2MeSADP/H_2O_2, Student's t-test). Results were expressed as means + SEM of triplicate measurements ($n = 3$).

TABLE 1. List of PTP Genes Upregulated by ATP in Astrocytes

Title	Fold increase (RT-PCR)	Gene ontology*
Protein tyrosine phosphatase 4a1	1.7 (5.7)	Protein tyrosine phosphatase activity (GO:0004725) Nucleus (GO:0005634)
Protein tyrosine phosphatase, receptor type, O	1.8 (4.4)	Protein tyrosine phosphatase activity (GO:0004725) Nervous system development (GO:0007399)
	1.6	Protein tyrosine phosphatase activity (GO:0004725) Nervous system development (GO:0007399)

*GO ontology defined by Gene Ontology Consortium (www.godatabase.org/cgi-bin/amigo/go.cgi).

(Heffetz et al., 1990; Shisheva and Shechter, 1993) on the ATP- and 2MeSADP-induced cytoprotective action in astrocytes. Na_3VO_4 concentration-dependently reversed the cytoprotective effect by ATP and 2MeSADP against H_2O_2 (Fig. 7B). Na_3VO_4 alone did not affect the cell viability of the astrocytes (light gray column). Additionally, Na_3VO_4 also reversed the inhibition by ATP or 2MeSADP of the H_2O_2-evoked phosphorylation of ERK1/2 in astrocytes (Fig. 7C). Then, we studied the effect of the selective $P2Y_1$ receptor antagonist MRS2179 (10 μM) on the PTP activity. H_2O_2 decreased the PTP activity to about one half. 2MeSADP restored the PTP activity and this effect was reversed by MRS2179 [Fig. 7D(1)]. As previously reported, $P2Y_1$ receptor activation also upregulates oxidoreductases such as TrxR, thereby protecting astrocytes against H_2O_2 (Shinozaki et al., 2005). The TrxR inhibitor auranofin (1 μM) also reversed the 2MeSADP-restored PTP activity. Furthermore, the thiol-containing antioxidant *N*-acetyl cystein (NAC, 10 mM) restored the H_2O_2-decreased PTP activity. In addition, we studied the effect of 2MeSADP, MRS2179 (10 μM), auranofin (1 μM), and NAC (10 mM) on the H_2O_2-evoked ERK1/2 activation [Fig. 7D(2)]. The inhibition of P-ERK1/2 activation by 2MeSADP (1 μM) was reversed by MRS2179 (10 μM) and auranofin (1 μM). In contrast, the H_2O_2-evoked ERK1/2 activation was prevented by NAC (10 mM). MRS2179 was added to the cells 1 h before the 2MeSADP treatment. Auranofin and NAC were added to the cells 1 h before H_2O_2 stimulation.

Involvement of src Tyrosine Kinase Family on H_2O_2-Evoked Cell Death and ERK1/2 Activation

Using Western blotting analysis, we studied whether H_2O_2 induces protein tyrosine phosphorylation. H_2O_2 evoked protein tyrosine phosphorylation, which was inhibited by pretreatment with ATP (100 μM, 24 h) or 2MeSADP (1 μM, 24 h) (Fig. 8A). This ATP- and

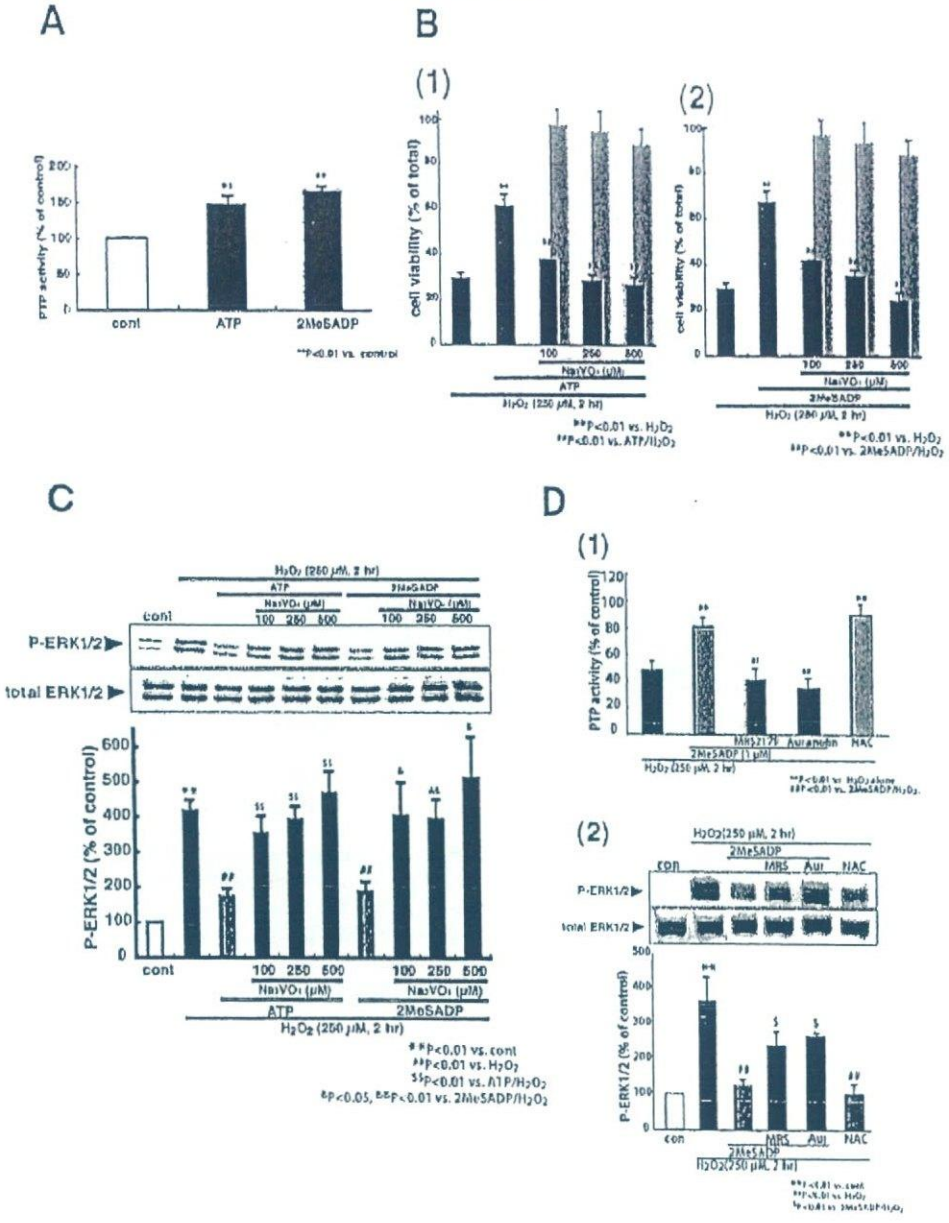

Fig. 7. The effect of ATP-induced PTP upregulation on H_2O_2-evoked cell death and ERK1/2 activation. A: ATP- and 2MeSADP-induced an increase of the PTP activity. ATP (100 μM, 24 h) and 2MeSADP (1 μM, 24 h) significantly increased the PTP activity (ATP: 148.3% ± 8.8%; 2MeSADP: 168.8% ± 4.8%, vs. control). Asterisks show significant difference from control ($^{**}P < 0.01$ vs. control, Student's *t*-test). B: PTP participates in ATP- and 2MeSADP-induced cytoprotective effect. The PTP inhibitor Na_3VO_4 (100–500 μM, 1 h) reversed the ATP(100 μM, 24 h)- and 2MeSADP(1 μM, 24 h)-induced protective effect concentration-dependently (black column). Na_3VO_4 alone did not affect the cell viability of the astrocytes (light gray column). Asterisks show significant difference from the response evoked by H_2O_2 ($^{**}P < 0.01$ vs. 250 μM H_2O_2, Student's *t*-test). Sharps show significant difference from the response by ATP/H_2O_2 or 2MeSADP/H_2O_2 ($^{\#\#}P < 0.01$ vs. ATP/H_2O_2 or 2MeSADP/H_2O_2, Student's *t*-test). C: PTP participates in ATP- and 2MeSADP-induced inhibition of H_2O_2-evoked ERK1/2 activation. Na_3VO_4 (100–500 μM, 1 h) reversed the ATP(100 μM, 24 h)- and 2MeSADP(1 μM, 24 h)-induced inhibition of H_2O_2-evoked ERK1/2 activation. The cells were treated with ATP and 2MeSADP 24 h before and during H_2O_2 treatment. Na_3VO_4 was added to the cells 1 h before the H_2O_2 (250 μM) treatment. Asterisks show significant difference from control ($^{**}P < 0.01$ vs. control, Student's *t*-test). Sharps show significant difference from H_2O_2 ($^{\#\#}P < 0.01$ vs. H_2O_2, Student's *t*-test). Dollar marks show significant difference from ATP/H_2O_2 or 2MeSADP/H_2O_2 ($^{\$}P < 0.05$, $^{\$\$}P < 0.01$ vs. ATP/H_2O_2 or 2MeSADP/H_2O_2, Student's *t*-test). D: The effect of MRS2179, auranofin, and NAC on PTP and ERK1/2 activity. (1) 2MeSADP (1 μM) restored the H_2O_2 (250 μM, 2 h)-decreased PTP activity and the effect was reversed by MRS2179 (10 μM) and auranofin (1 μM). NAC (10 mM) restored the PTP activity decreased by H_2O_2. Asterisks show significant difference from the response evoked by H_2O_2 ($^{**}P < 0.01$ vs. 250 μM H_2O_2, Student's *t*-test). Sharps show significant difference from the response by 2MeSADP/H_2O_2 ($^{\#\#}P < 0.01$ vs. 2MeSADP/H_2O_2). (2) The effect of MRS2179, auranofin, and NAC on H_2O_2-evoked ERK1/2 activation. MRS2179 (10 μM) and auranofin (1 μM) reversed the ERK1/2 activity inhibited by 2MeSADP. NAC (10 mM) prevented the H_2O_2-evoked ERK1/2 activation. Asterisks show significant difference from control ($^{**}P < 0.01$ vs. control, Student's *t*-test). Sharps show significant difference from H_2O_2 ($^{\#\#}P < 0.01$ vs. H_2O_2, Student's *t*-test). Dollar marks show significant difference from 2MeSADP/H_2O_2 ($^{\$}P < 0.05$ vs. 2MeSADP/H_2O_2, Student's Results were expressed as means *t*-test). Results were expressed as means ± SEM of triplicate measurements ($n = 3$).

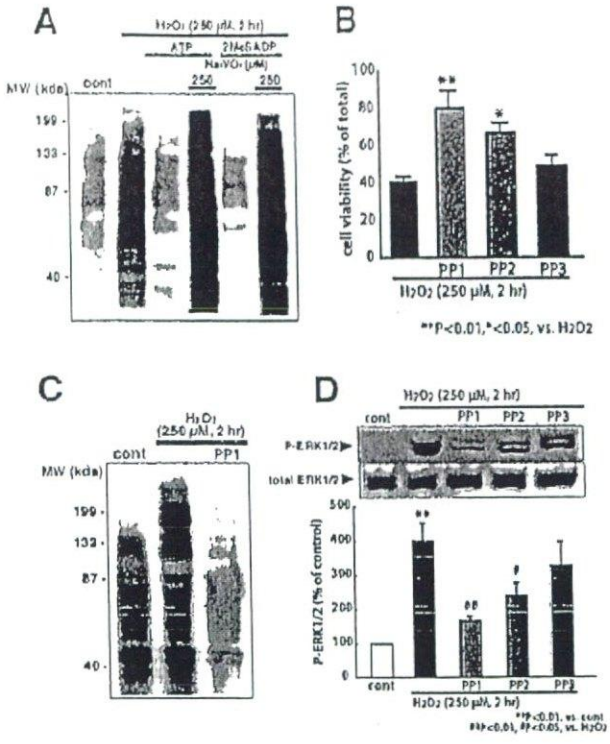

Fig. 8. The effects of the src family on the H_2O_2-evoked cell death and ERK1/2 activation. A: ATP and 2MeSADP prevented the H_2O_2-evoked protein tyrosine phosphorylation via PTP upregulation. H_2O_2 (250 μM) evoked the protein tyrosine phosphorylation. Na_3VO_4 (250 μM) markedly inhibited the ATP-(100 μM, 24 h) and 2MeSADP (1 μM, 24 h)-induced prevention of the H_2O_2-evoked protein tyrosine phosphorylation. Na_3VO_4 was applied to the cells 1 h before and during the H_2O_2 treatment. B: The effect of selective src family inhibitors on the H_2O_2-evoked cell death. PP1 and PP2 (250 nM) prevented the H_2O_2-evoked cell death but PP3 (250 nM) did not. Asterisks show significant difference from the response evoked by H_2O_2 ($^*P < 0.05$, $^{**}P < 0.01$ vs. 250 μM H_2O_2, Student's *t*-test). C: The effect of PP1 on H_2O_2-evoked protein tyrosine phosphorylation. PP1 (250 nM) strongly inhibited the H_2O_2-evoked protein tyrosine phosphorylation. D: The effect of selective src family inhibitors on H_2O_2-evoked ERK1/2 activation. PP1 and PP2 (250 nM) inhibited H_2O_2-evoked ERK1/2 activation but PP3 (250 nM) did not. PP1, PP2, and PP3 were applied to the cells 1 h before and during the H_2O_2 treatment. Asterisks show significant difference from control ($^{**}P < 0.01$ vs. control, Student's *t*-test). Sharps show significant difference from H_2O_2 ($^{\#\#}P < 0.01$ vs. H_2O_2, Student's *t*-test). Results were expressed as means ± SEM of triplicate measurements ($n = 3$).

2MeSADP-induced prevention disappeared when the astrocytes were treated with Na_3VO_4 to inhibit the PTP activity, suggesting that ATP and 2MeSADP would inhibit tyrosine phosphorylation through a pathway(s) mediated by PTP. As it has been reported that H_2O_2 especially activates the src tyrosine kinase family of PTK (Lee and Esselman, 2002; Nishida et al., 2000), we pharmacologically studied whether the src family participates in the H_2O_2-evoked cell death and ERK1/2 activation. When the selective src family inhibitors PP1 (250 nM) and PP2 (250 nM) (Hanke et al., 1996) were added to the cells 1 h before H_2O_2 treatment, the H_2O_2-evoked cell death in astrocytes was abolished (Fig. 8B). The inactive analogue PP3 (250 nM) did not inhibit the H_2O_2-evoked cell death. PP1 (250 nM) also inhibited the H_2O_2-evoked protein tyrosine phosphorylation (Fig. 8C). In addition, the H_2O_2-evoked ERK1/2 activation was inhibited by PP1 and PP2 (250 nM) but not by PP3 (Fig. 8D). PP1, PP2, and PP3 were added to the cells 1 h before H_2O_2 stimulation.

DISCUSSION

In the present study, we demonstrated that ERK1/2 and src family are important molecules that promote the H_2O_2-evoked astrocytic cell death, and that ATP upregulates PTP expression and its activity, thereby preventing the H_2O_2-evoked src family and following ERK1/2 activation, resulting in the protection of astrocytes against H_2O_2-evoked cell death.

We clearly showed that the H_2O_2-evoked activation of ERK1/2 and accumulation of P-ERK in nuclei were critical events that promote cell death in astrocytes. ATP itself, however, which exhibited a protective effect against H_2O_2 in our study, is also known to activate ERK1/2 in astrocytes (Neary et al., 1999, 2003; Panenka et al., 2001). In fact, ATP and 2MeSADP activated ERK1/2 in astrocytes. However, the ERK1/2 activation by ATP, in contrast to that by H_2O_2, was transient (5–15 min after stimulation) and did not affect the astrocyte cell viability. Furthermore, 2MeSADP-activated ERK1/2 seems to function rather as an essential signal that prevents cell death and induces the upregulation of oxidoreductases and PTP gene expression. Thus, such a discrepancy appears to result from spatio- and temporal-behavioral differences of P-ERK1/2. It is known that, after faint brain ischemia, neuronal cells acquire tolerance to a subsequent more serious ischemic injury (Chen and Simon, 1997; Dawson and Dawson, 2000; Schaller and Graf, 2002). The similarity between such preconditioning against ischemia and the preconditioning of ERK1/2 against H_2O_2-evoked cell death is very interesting.

In the present study, the extent of the ERK1/2 activity appeared to be important in the H_2O_2-evoked cell death because of the correspondence between the concentration-dependency of the H_2O_2-evoked ERK1/2 activity and that of the H_2O_2-evoked cell death (Shinozaki et al., 2005). Although recent studies also have reported that H_2O_2-activated ERK1/2 evokes cell death in glioma and osteoblastic cells (Choi et al., 2005; Levinthal and Defranco, 2005), the spatio- and temporal behavior of P-ERK1/2 remained unclear. P-ERK1/2 is known to translocate into the nucleus (Rosenberger et al., 2001) and accumulate there (Brand et al., 2001; Stanciu and DeFranco, 2002), thereby inducing neuronal death. In the immunocytochemical analysis, stimulation by 250 μM but not by 50 μM H_2O_2 for 2 h induced P-ERK1/2 accumulation in the nucleus. Most of the total ERK1/2 existed in the cytoplasm and was not affected by H_2O_2 (50 or 250 μM). Accordingly, it is conceivable that only P-ERK1/2, activated by high concentrations (i.e. 250 μM) of H_2O_2, accumulates in the nucleus and induces cell

death. In a spatiotemporal analysis of P-ERK1/2, although there was a time-dependent activation of ERK1/2 by 50 and 250 μM H_2O_2 at the whole cell level, the fraction of N = E was increased transiently (~15 min after stimulation) by 50 μM H_2O_2 but time-dependently by 250 μM. These results suggest that the long-term accumulation of P-ERK1/2 into the nucleus participates in the H_2O_2-evoked cell death.

In physiological conditions, it is suggested that the P-ERK1/2 translocated into the nucleus is dephosphorylated by MAPK phosphatase (MAPKP), especially by the ERK1/2 selective phosphatase MAPK phosphatase-3 (MKP-3) (Dowd et al., 1998; Groom et al., 1996) and is exported from the nucleus depending on MKP-3 (Karlsson et al., 2004). The interaction between MKP-3 and ERK1/2 requires arginine residues of MKP-3 (Nichols et al., 2000). Because many amino acids, including arginines, in protein are oxidized by H_2O_2 (Amici et al., 1989; Moskovitz et al., 2002; Stadtman and Berlett, 1997; Taborsky, 1973), the interaction of MKP-3 and ERK1/2 and the nuclear export of ERK1/2 may be affected by H_2O_2. Furthermore, the ERK1/2 inactivating enzyme MAPKP is inactivated by H_2O_2 (Foley et al., 2004; Levinthal and Defranco, 2005). In conditions with oxidative stress, it is conceivable that the dephosphorylation and nuclear export of activated-ERK1/2 are attenuated because of the decreased MAPKP function and the association between MAPKP and ERK1/2, which thereby induces the prolonged activation and nuclear accumulation of ERK1/2.

With regard to the upstream molecule that activates ERK1/2 in response to H_2O_2, we found that the src family is important. Furthermore, we demonstrated that activation of $P2Y_1$ receptors inhibits the activation of src family and subsequent signaling cascades by upregulating the PTP expression and activity. We previously reported that ATP upregulates the thiol-containing protein TrxR (Shinozaki et al., 2005). The enzymatic activity of PTP requires reduction of the cystein residue in its active center (Cho et al., 2004; Persson et al., 2004). Accordingly, the redox state of the cystein residue in PTP is considered to crucially affect its phosphatase activity. The decreased activity of PTP in an oxidative state is recovered by adding thiol-containing protein such as glutathione (Salmeen et al., 2003) and thioredoxin (Lee and Esselman, 2002). In fact, the $P2Y_1$ receptor activation-induced restoration of the PTP activity was reversed by auranofin, indicating that TrxR restores the PTP activity. Additionally, the antioxidant NAC restored the PTP activity decreased by H_2O_2 (250 μM). The protective effect of PTP induced by ATP requires either an increase in the amount/activity of PTP or a reduction, in which the upregulated TxrR would have a critical role (Shinozaki et al., 2005). Furthermore, such ATP-induced oxidoreductases may preserve the MKP-3 activity, thereby enhancing the dephosphorylation and inactivation of ERK1/2 and the nuclear export of ERK1/2.

PTP and PTK regulate protein tyrosine phosphorylation in close coordination with each other. ATP prevented the H_2O_2-induced protein tyrosine phosphorylation by increasing the PTP activity. The inhibition of the H_2O_2-evoked cell death by PP1 and PP2 and the tyrosine phosphorylation by PP1 indicates that the src tyrosine kinase family is related to the H_2O_2-evoked cell death. Additionally, PP1 and PP2 inhibited the H_2O_2-evoked ERK1/2 activation, indicating that ERK1/2 is activated following src family activation. As the src family is activated by cystein oxidation independently of tyrosine phosphorylation (Akhand et al., 1999; Pu et al., 1996), under oxidative stress such as by H_2O_2 treatment or in condition of ischemia/reperfusion-injury, the src family could be activated independent of tyrosine phosphorylation. In contrast to src activation, PTP and MAPKP are inactivated by oxidation of the cystein residue under oxidative conditions (Cho et al., 2004; Foley et al., 2004; Meng et al., 2004). Briefly, the "irresponsive to control" signal transduction could be caused under oxidative conditions.

In conclusion, we clearly demonstrated that the src family activation followed by strong ERK1/2 activation and prolonged P-ERK1/2 accumulation into the nucleus participated in the H_2O_2-evoked cell death of astrocytes. $ATP/P2Y_1$ receptor activation inhibits H_2O_2-evoked ERK1/2 activation by preventing the H_2O_2-evoked src activation via upregulation of PTP expression/activity. Our present findings suggest that the gliotransmitter ATP protects astrocytes against oxidative stress by counteracting the intracellular signaling pathway that evokes cell death.

ACKNOWLEDGMENTS

We thank Tomoko Obama for technical assistance.

REFERENCES

Akhand AA, Pu M, Senga T, Kato M, Suzuki H, Miyata T, Hamaguchi M, Nakashima I. 1999. Nitric oxide controls src kinase activity through a sulfhydryl group modification-mediated Tyr-527-independent and Tyr-416-linked mechanism. J Biol Chem 274:25821–25826.

Alessandrini A, Namura S, Moskowitz MA, Bonventre JV. 1999. MEK1 protein kinase inhibition protects against damage resulting from focal cerebral ischemia. Proc Natl Acad Sci USA 96:12866–12869.

Alessi DR, Cuenda A, Cohen P, Dudley DT, Saltiel AR. 1995. PD 098059 is a specific inhibitor of the activation of mitogen-activated protein kinase kinase in vitro and in vivo. J Biol Chem 270:27489–27494.

Amici A, Levine RL, Tsai L, Stadtman ER. 1989. Conversion of amino acid residues in proteins and amino acid homopolymers to carbonyl derivatives by metal-catalyzed oxidation reactions. J Biol Chem 264:3341–3346.

Bennett BL, Sasaki DT, Murray BW, O'Leary EC, Sakata ST, Xu W, Leisten JC, Motiwala A, Pierce S, Satoh Y, Bhagwat SS, Manning AM, Anderson DW. 2001. SP600125, an anthrapyrazolone inhibitor of Jun N-terminal kinase. Proc Natl Acad Sci USA 98:13681–13686.

Boschert U, Muda M, Camps M, Dickinson R, Arkinstall S. 1997. Induction of the dual specificity phosphatase PAC1 in rat brain following seizure activity. Neuroreport 8:3077–3080.

Boulton TG, Nye SH, Robbins DJ, Ip NY, Radziejewska E, Morgenbesser SD, DePinho RA, Panayotatos N, Cobb MH, Yancopoulos GD. 1991. ERKs: A family of protein-serine/threonine kinases that are activated and tyrosine phosphorylated in response to insulin and NGF. Cell 65:663–675.

Brand A, Gil S, Seger R, Yavin E. 2001. Lipid constituents in oligodendroglial cells alter susceptibility to H_2O_2-induced apoptotic cell death via ERK activation. J Neurochem 76:910–918.

Brugge JS, Cotton PC, Queral AE, Barrett JN, Nonner D, Keane RW. 1985. Neurones express high levels of a structurally modified, activated form of pp60c-src. Nature 316:554–557.

Chen J, Simon R. 1997. Ischemic tolerance in the brain. Neurology 48:306–311.
Chen RH, Sarnecki C, Blenis J. 1992. Nuclear localization and regulation of erk- and rsk-encoded protein kinases. Mol Cell Biol 12:915–927.
Cho SH, Lee CH, Ahn Y, Kim H, Ahn CY, Yang KS, Lee SR. 2004. Redox regulation of PTEN and protein tyrosine phosphatases in H_2O_2-mediated cell signaling. FEBS Lett 560(1–3):7–13.
Choi JS, Park HJ, Kim HY, Kim SY, Lee JE, Choi YS, Chun MH, Chung JW, Lee MY. 2005. Phosphorylation of PTEN and Akt in astrocytes of the rat hippocampus following transient forebrain ischemia. Cell Tissue Res 319:359–366.
Dawson VL, Dawson TM. 2000. Neuronal ischaemic preconditioning. Trends Pharmacol Sci 21:423–424.
Dowd S, Sneddon AA, Keyse SM. 1998. Isolation of the human genes encoding the pyst1 and Pyst2 phosphatases: Characterisation of Pyst2 as a cytosolic dual-specificity MAP kinase phosphatase and its catalytic activation by both MAP, SAP kinases. J Cell Sci 111(Part 22):3389–3399.
Fam SR, Gallagher CJ, Salter MW. 2000. P2Y(1) purinoceptor-mediated Ca(2+) signaling and Ca(2+) wave propagation in dorsal spinal cord astrocytes. J Neurosci 20:2800–2808.
Favata MF, Horiuchi KY, Manos EJ, Daulerio AJ, Stradley DA, Feeser WS, Van Dyk DE, Pitts WJ, Earl RA, Hobbs F, Copeland RA, Magolda RL,Scherle PA, Trzaskos JM. 1998. Identification of a novel inhibitor of mitogen-activated protein kinase kinase. J Biol Chem 273:18623–18632.
Fialkow L, Chan CK, Rotin D, Grinstein S, Downey GP. 1994. Activation of the mitogen-activated protein kinase signaling pathway in neutrophils. Role of oxidants. J Biol Chem 269:31234–31242.
Fields RD, Stevens-Graham B. 2002. New insights into neuron-glia communication. Science 298:556–562.
Foley TD, Armstrong JJ, Kupchak BR. 2004. Identification and H_2O_2 sensitivity of the major constitutive MAPK phosphatase from rat brain. Biochem Biophys Res Commun 315:568–574.
Gonzalez FA, Seth A, Raden DL, Bowman DS, Fay FS, Davis RJ. 1993. Serum-induced translocation of mitogen-activated protein kinase to the cell surface ruffling membrane and the nucleus. J Cell Biol 122:1089–1101.
Groom LA, Sneddon AA, Alessi DR, Dowd S, Keyse SM. 1996. Differential regulation of the MAP, SAP and RK/p38 kinases by Pyst1, a novel cytosolic dual-specificity phosphatase. EMBO J 15:3621–3632.
Guo J, Meng F, Zhang G, Zhang Q. 2003. Free radicals are involved in continuous activation of nonreceptor tyrosine protein kinase c-Src after ischemia/reperfusion in rat hippocampus. Neurosci Lett 345:101–104.
Guyton KZ, Liu Y, Gorospe M, Xu Q, Holbrook NJ. 1996. Activation of mitogen-activated protein kinase by H_2O_2. Role in cell survival following oxidant injury. J Biol Chem 271:4138–4142.
Hanke JH, Gardner JP, Dow RL, Changelian PS, Brissette WH, Weringer EJ, Pollok BA, Connelly PA. 1996. Discovery of a novel, potent, and Src family-selective tyrosine kinase inhibitor. Study of Lck- and FynT-dependent T cell activation. J Biol Chem 271:695–701.
Hansson E, Ronnback L. 2003. Glial neuronal signaling in the central nervous system. FASEB J 17:341–348.
Heffetz D, Bushkin I, Dror R, Zick Y. 1990. The insulinomimetic agents H_2O_2 and vanadate stimulate protein tyrosine phosphorylation in intact cells. J Biol Chem 265:2896–2902.
Inoue K. 2002. Microglial activation by purines and pyrimidines. Glia 40:156–163.
Karlsson M, Mathers J, Dickinson RJ, Mandl M, Keyse SM. 2004. Both nuclear-cytoplasmic shuttling of the dual specificity phosphatase MKP-3 and its ability to anchor MAP kinase in the cytoplasm are mediated by a conserved nuclear export signal. J Biol Chem 279:41882–41891.
Kimura M, Maeda K, Hayashi S. 1992. Cytosolic calcium increase in coronary endothelial cells after H_2O_2 exposure and the inhibitory effect of U78517F. Br J Pharmacol 107:488–493.
Konishi H, Matsuzaki H, Tanaishi H, Yamamoto T, Fukunaga M, Ono Y, Kikkawa U. 1999. Opposing effects of protein kinase C δ and protein kinase B α on H_2O_2-induced apoptosis in CHO cells. Biochem Biophys Res Commun 264:840–846.
Lee K, Esselman WJ. 2002. Inhibition of PTPs by H_2O_2 regulates the activation of distinct MAPK pathways. Free Radic Biol Med 33:1121–1132.
Levinthal DJ, Defranco DB. 2005. Reversible oxidation of ERK-directed protein phosphatases drives oxidative toxicity in neurons. J Biol Chem 280:5875–5883.
Marshall CJ. 1995. Specificity of receptor tyrosine kinase signaling: Transient versus sustained extracellular signal-regulated kinase activation. Cell 80:179–185.
McLaughlin MM, Kumar S, McDonnell PC, Van Horn S, Lee JC, Livi GP, Young PR. 1996. Identification of mitogen-activated protein (MAP) kinase-activated protein kinase-3, a novel substrate of CSBP p38 MAP kinase. J Biol Chem 271:8488–8492.
Meng TC, Buckley DA, Galic S, Tiganis T, Tonks NK. 2004. Regulation of insulin signaling through reversible oxidation of the protein-tyrosine phosphatases TC45 and PTP1B. J Biol Chem 279:37716–37725.
Moskovitz J, Yim MB, Chock PB. 2002. Free radicals and disease. Arch Biochem Biophys 397:354–359.
Murray B, Alessandrini A, Cole AJ, Yee AG, Furshpan EJ. 1998. Inhibition of the p44/42 MAP kinase pathway protects hippocampal neurons in a cell-culture model of seizure activity. Proc Natl Acad Sci USA 95:11975–11980.
Namura S, Iihara K, Takami S, Nagata I, Kikuchi H, Matsushita K, Moskowitz MA, Bonventre JV, Alessandrini A. 2001. Intravenous administration of MEK inhibitor U0126 affords brain protection against forebrain ischemia and focal cerebral ischemia. Proc Natl Acad Sci USA 98:11569–11574.
Neary JT, Kang Y, Bu Y, Yu E, Akong K, Peters CM. 1999. Mitogenic signaling by ATP/P2Y purinergic receptors in astrocytes: Involvement of a calcium-independent protein kinase C, extracellular signal-regulated protein kinase pathway distinct from the phosphatidylinositol-specific phospholipase C/calcium pathway. J Neurosci 19:4211–4220.
Neary JT, Kang Y, Willoughby KA, Ellis EF. 2003. Activation of extracellular signal-regulated kinase by stretch-induced injury in astrocytes involves extracellular ATP, P2 purinergic receptors. J Neurosci 23:2348–2356.
Nichols A, Camps M, Gillieron C, Chabert C, Brunet A, Wilsbacher J, Cobb M, Pouyssegur J, Shaw JP, Arkinstall S. 2000. Substrate recognition domains within extracellular signal-regulated kinase mediate binding and catalytic activation of mitogen-activated protein kinase phosphatase-3. J Biol Chem 275:24613–24621.
Nishida M, Maruyama Y, Tanaka R, Kontani K, Nagao T, Kurose H. 2000. G α(i) and G α(o) are target proteins of reactive oxygen species. Nature 408:492–495.
Ohtsuki T, Matsumoto M, Kitagawa K, Mabuchi T, Mandai K, Matsushita K, Kuwahara K, Tagaya M, Ogawa S, Ueda H, Kamada T, Yanagihara T. 1996. Delayed neuronal death in ischemic hippocampus involves stimulation of protein tyrosine phosphorylation. Am J Physiol 271(4, Part 1):C1085–C1097.
Oppenheim RW. 1991. Cell death during development of the nervous system. Annu Rev Neurosci 14:453–501.
Panenka W, Jijon H, Herx LM, Armstrong JN, Feighan D, Wei T, Yong VW, Ransohoff RM, MacVicar BA. 2001. P2X7-like receptor activation in astrocytes increases chemokine monocyte chemoattractant protein-1 expression via mitogen-activated protein kinase. J Neurosci 21:7135–7142.
Persson C, Sjoblom T, Groen A, Kappert K, Engstrom U, Hellman U, Heldin CH, den Hertog J, Ostman A. 2004. Preferential oxidation of the second phosphatase domain of receptor-like PTP-α revealed by an antibody against oxidized protein tyrosine phosphatases. Proc Natl Acad Sci USA 101:1886–1891.
Pu M, Akhand AA, Kato M, Hamaguchi M, Koike T, Iwata H, Sabe H, Suzuki H, Nakashima I. 1996. Evidence of a novel redox-linked activation mechanism for the Src kinase which is independent of tyrosine 527-mediated regulation. Oncogene 13:2615–2622.
Rosenberger J, Petrovics G, Buzas B. 2001. Oxidative stress induces proorphanin FQ, proenkephalin gene expression in astrocytes through p38- and ERK-MAP kinases and NF-κB. J Neurochem 79:35–44.
Salmeen A, Andersen JN, Myers MP, Meng TC, Hinks JA, Tonks NK, Barford D. 2003. Redox regulation of protein tyrosine phosphatase 1B involves a sulphenyl-amide intermediate. Nature 423:769–773.
Schaller B, Graf R. 2002. Cerebral ischemic preconditioning. An experimental phenomenon or a clinical important entity of stroke prevention? J Neurol 249:1503–1511.
Segal RA, Greenberg ME. 1996. Intracellular signaling pathways activated by neurotrophic factors. Annu Rev Neurosci 19:463–489.
Shinozaki Y, Koizumi S, Ishida S, Sawada JI, Ohno Y, Inoue K. 2005. Cytoprotection against oxidative stress-induced damage of astrocytes by extracellular ATP via P2Y(1) receptors. Glia 49:288–300.
Shisheva A, Shechter Y. 1993. Role of cytosolic tyrosine kinase in mediating insulin-like actions of vanadate in rat adipocytes. J Biol Chem 268:6463–6469.
Stadtman ER, Berlett BS. 1997. Reactive oxygen-mediated protein oxidation in aging and disease. Chem Res Toxicol 10:485–494.
Stanciu M, DeFranco DB. 2002. Prolonged nuclear retention of activated extracellular signal-regulated protein kinase promotes cell death generated by oxidative toxicity or proteasome inhibition in a neuronal cell line. J Biol Chem 277:4010–4017.
Subramaniam S, Zirrgiebel U, Von Bohlen Und Halbach O, Strelau J, Laliberte C, Kaplan DR, Unsicker K. 2004. ERK activation promotes neuronal degeneration predominantly through plasma membrane damage and independently of caspase-3. J Cell Biol 165:357–369.

Sugrue MM, Brugge JS, Marshak DR, Greengard P, Gustafson EL. 1990. Immunocytochemical localization of the neuron-specific form of the c-src gene product, pp60c-src(+), in rat brain. J Neurosci 10:2513–2527.

Taborsky G. 1973. Oxidative modification of proteins in the presence of ferrous ion and air. Effect of ionic constituents of the reaction medium on the nature of the oxidation products. Biochemistry 12:1341–1348.

Takahashi M, Berk BC. 1996. Mitogen-activated protein kinase (ERK1/2) activation by shear stress and adhesion in endothelial cells. Essential role for a herbimycin-sensitive kinase. J Clin Invest 98:2623–2631.

Takano S, Fukuyama H, Fukumoto M, Kimura J, Xue JH, Ohashi H, Fujita J. 1996. PRL-1, a protein tyrosine phosphatase, is expressed in neurons and oligodendrocytes in the brain and induced in the cerebral cortex following transient forebrain ischemia. Brain Res Mol Brain Res 40:105–115.

Tan J, Town T, Mori T, Wu Y, Saxe M, Crawford F, Mullan M. 2000. CD45 opposes β-amyloid peptide-induced microglial activation via inhibition of p44/42 mitogen-activated protein kinase. J Neurosci 20:7587–7594.

Ushio-Fukai M, Alexander RW, Akers M, Yin Q, Fujio Y, Walsh K, Griendling KK. 1999. Reactive oxygen species mediate the activation of Akt/protein kinase B by angiotensin II in vascular smooth muscle cells. J Biol Chem 274:22699–22704.

Wang X, Martindale JL, Liu Y, Holbrook NJ. 1998. The cellular response to oxidative stress: Influences of mitogen-activated protein kinase signalling pathways on cell survival. Biochem J 333(Part 2):291–300.

Xia Z, Dickens M, Raingeaud J, Davis RJ, Greenberg ME. 1995. Opposing effects of ERK, JNK-p38 MAP kinases on apoptosis. Science 270:1326–1331.

Yu XM, Salter MW. 1999. Src, a molecular switch governing gain control of synaptic transmission mediated by *N*-methyl-D-aspartate receptors. Proc Natl Acad Sci USA 96:7697–7704.

0026-895X/06/7001-319-328$20.00
MOLECULAR PHARMACOLOGY

Mol Pharmacol 70:319–328, 2006

Vol. 70, No. 1
20511/3124430
Printed in U.S.A.

Retinoic Acids Increase $P2X_2$ Receptor Expression through the 5′-Flanking Region of *P2rx2* Gene in Rat Phaeochromocytoma PC-12 Cells

Hidetoshi Tozaki-Saitoh, Schuichi Koizumi, Yoji Sato, Makoto Tsuda, Taku Nagao, and Kazuhide Inoue

Divisions of Pharmacology (H.T.-S., S.K.) and Cellular and Gene Therapy Products (Y.S.), National Institute of Health Sciences, Tokyo, Japan; National Institute of Health Sciences, Tokyo, Japan (T.N.); and Department of Molecular and System Pharmacology, Graduate School of Pharmaceutical Sciences, Kyushu University, Fukuoka, Japan (H.T.-S., M.T., K.I.)

Received November 1, 2005; accepted April 25, 2006

ABSTRACT

The $P2X_2$ receptor is a subtype of ionotropic ATP receptor and plays a significant role in regulating fast synaptic transmission in the nervous system. Because the expression level of the $P2X_2$ receptor is known to determine its channel properties and functional interactions with other neurotransmitter channels, elucidating the mechanisms underlying the regulation of $P2X_2$ receptor expression in neuronal cells is important. Here, we identified three motifs that correspond to the retinoic acid response element in the 5′-flanking region of the rat $P2X_2$ gene. In rat pheochromocytoma PC-12 cells, treatment with 9-*cis*-retinoic acid as well as all-*trans*-retinoic acid significantly increased the mRNA and protein level of $P2X_2$ receptor. In addition, in PC-12 cells transiently transfected with a luciferase reporter gene driven by the promoter region of the rat $P2X_2$ gene, both 9-*cis*-retinoic acid and all-*trans*-retinoic acid increased the luciferase activity, whereas their effects were diminished by truncation of the retinoic acid response elements in the promoter. Furthermore, 9-*cis*-retinoic acid enhanced the ATP-evoked whole cell currents and intracellular Ca^{2+}- and ATP-evoked dopamine release, indicating the up-regulation of functional $P2X_2$ receptors on the plasma membrane. These results provide the molecular mechanism underlying the transcriptional regulation of $P2X_2$ receptors and suggest that retinoid is an important factor in regulating $P2X_2$ receptors in the nervous system.

P2X receptors, of which seven subtypes ($P2X_1$–$P2X_7$) have so far been cloned, are a family of ligand-gated cation channels activated by extracellular ATP and are widely expressed in the peripheral and central nervous system (North, 2002; Illes and Alexandre Ribeiro, 2004). A growing body of evidence indicates that P2X receptors expressed in neurons play important roles in mediating (Galligan and Bertrand, 1994), facilitating presynaptically (Khakh et al., 2003; Shigetomi and Kato, 2004), and modulating postsynaptically fast excitatory and inhibitory synaptic transmission (Wang et al., 2004). It remains unclear which P2X receptor subtypes are the main targets for ATP at synapses, but several lines of evidence have suggested the $P2X_2$ receptor as a candidate. In several regions of the nervous system, neurons express functional $P2X_2$ receptors (North, 2002; Illes and Alexandre Ribeiro, 2004) as well as both the mRNA and protein of $P2X_2$ receptors (Kanjhan et al., 1999). An electron microscopic study has shown that $P2X_2$ receptors are localized at the postsynaptic membrane in the cerebellum and the CA1 region of the hippocampus (Rubio and Soto, 2001). In addition, it has been reported that $P2X_2$ receptors are abundant in the biochemically fractionated presynaptic active zone in the hippocampus (Rodrigues et al., 2005). A recent study has shown that ATP facilitates excitatory glutamate transmission onto stratum radiatum interneurons, a population of the ATP-

This work was partly supported by The National Institute of Biomedical Innovation (Medical Frontier Project; MF-16), The Health Science Foundation in Japan, and a grant-in-aid for scientific research from the Ministry of Education, Science, Sports and Culture.

Article, publication date, and citation information can be found at http://molpharm.aspetjournals.org.
doi:10.1124/mol.105.020511.

ABBREVIATIONS: RARE, retinoic acid response element; RAR, retinoic acid receptor; RXR, retinoid X receptor; DA, dopamine; VDCC, voltage-dependent calcium channel; RA, retinoic acid; RT-PCR, reverse transcriptase polymerase chain reaction; bp, base pair(s); PCR, polymerase chain reaction; TESS, transcription element search system; RACE, rapid amplification of cDNA ends; $P2X_2R$, $P2X_2$ receptor; GAPDH, glyceraldehyde-3-phosphate dehydrogenase; GFP, green fluorescent protein; BSS, balanced salt solution; PCA, perchloric acid; AP, adaptor protein; atRA, all-*trans*-retinoic acid; PPADS, pyridoxal phosphate-6-azophenyl-2′4′-disulfonic acid; U-73122, 1-[6-[[17β-methoxyestra-1,3,5(10)-trien-17-yl]amino]hexyl]-1*H*-pyrrole-2,5-dione; DR, direct repeat; ANOVA, analysis of variance.

responding neurons that is markedly reduced in hippocampus slices from $P2X_2$-deficient mice (Khakh et al., 2003). These results indicate that in several regions $P2X_2$ receptors localized at pre- and/or postsynapses regulate fast synaptic transmission. Furthermore, $P2X_2$ receptors are associated directly with other neurotransmitter channels such as nicotinic acetylcholine receptors, 5-hydroxytryptamine receptors or $GABA_A$ receptors, and activation of both receptors produces nonadditive cross-inhibitory responses (Khakh et al., 2000; Boue-Grabot et al., 2003). It is noteworthy that the functional interaction of $P2X_2$ receptors with other channels is decreased at lower densities of channel expression (Khakh et al., 2000), suggesting that their expression levels affect cellular events resulting from activation of $P2X_2$ receptors at synapses. In addition, the expression level of $P2X_2$ receptors also changes their channel properties (Fujiwara and Kubo, 2004). Moreover, an increase in the expression of $P2X_2$ receptors in neuronal cells has been implicated in the development of several pathological states such as brain ischemia and chronic pain (Xu and Huang, 2002; Cavaliere et al., 2003). Therefore, to understand the physiological and pathological roles of $P2X_2$ receptors in the functioning of the nervous system, it is of particular importance to determine how the expression of $P2X_2$ receptors is regulated in neuronal cells.

In the present study, we cloned the 5′-flanking region of the rat $P2X_2$ gene (*P2rx2*) and identified three sites corresponding to a motif of retinoic acid response element (RARE). RARE is a binding site of nuclear receptors, including retinoic acid receptor (RAR) and retinoid X receptor (RXR), and is required for the gene expression induced by retinoids (Chambon, 1996). We further found that retinoids increase both the mRNA and protein expression of the $P2X_2$ receptor and enhance release of the neurotransmitter dopamine (DA) evoked by ATP through activating $P2X_2$ receptors from rat pheochromocytoma PC-12 cells, a neuronal model (Shafer and Atchison, 1991). Therefore, these results suggest that retinoids are regulators of the expression of $P2X_2$ receptors in neuronal cells in the nervous system.

Materials and Methods

PC-12 Cells. PC-12 cells (passage 55–70) were cultured according to Inoue and Kenimer (1988), and undifferentiated cells were used. Cells were cultured in Dulbecco's modified eagle's medium supplemented with 7.5% fetal bovine serum, 7.5% horse serum, and 4 mM L-glutamine. For reverse transcription-polymerase chain reaction (RT-PCR) and Western blot experiments, cells were plated on 60-mm collagen (Virtogen-100)-coated dishes for 2 days. For whole cell patch-clamp recording and intracellular calcium imaging, cells were plated on collagen-coated coverslips placed on the bottom of 35-mm polystyrene dishes. For the measurement of DA release, cells were plated on collagen-coated 35-mm polystyrene dishes.

Cloning of the $P2X_2$ Upstream Region. Sequences for the 5′-flanking region of *P2rx2* were obtained from National Center for Biotechnology Information Rat Genome Resources. The genomic 2.5-kb upstream sequence of the putative Wistar rat *P2rx2* transcription starting site was targeted as $P2X_2$ mRNA (GenBank accession number NM_053656) upstream sequence. The following primers were designed for amplification of the 5′-flanking region of *P2rx2*: forward primer, GAACCTCGAGTGAGCCACAACCAGAACACT; reverse primer, GACAAGATCTATGGCCCAAGGAGCTCGGT. Genomic DNA extracted from the tail of a female Wistar rat was used for the polymerase chain reaction. Four individual reactions were carried out, and amplicons were inserted in a pGEM-T vector (Promega, Madison, WI) for sequencing. Each insert was sequenced, and the exact sequence was estimated by comparing the four sequences. The relative location of the cloned sequence is confirmed to be just upstream of the first exon of *P2rx2* without any intervening inserts. Using primers specific to the third exon of *P2rx2* and −164 position of the cloned sequence, approximately 750-bp single-band amplification was obtained by PCR. This amplicon included the sequence comprising the 5′ site of $P2X_2$ mRNA (RefSeq sequence NM_053656) exactly as published, and the sequence was determined to be the 5′-flanking region without any additional intervening sequence. The sequence data from the 5′-flanking region of *P2rx2* has been deposited in GenBank with the accession number AY749416. Putative sites for the transcription element were analyzed using Transcription Element Search System (TESS) site (http://www.cbil.upenn.edu/tess).

"Oligo-Capping" 5′ Rapid Amplification of cDNA Ends of $P2X_2$ mRNA. Modified rapid amplification of 5′ cDNA ends (5′ RACE) was performed according to oligo-capping method developed by Maruyama and Sugano (1994). Total RNA (5 μg) extracted from PC-12 cells was treated with 1 unit of bacterial alkaline phosphatase (Takara, Kyoto, Japan) in supplied buffer with 100 units of RNase inhibitor (Toyobo, Osaka, Japan) at 37°C for 30 min to hydrolyze the phosphate of truncated mRNA 5′ ends. After extraction with phenol/chloroform (1:1) twice, chloroform once, and ethanol precipitation, tobacco acid pyrophosphatase (20 units; Wako Pure Chemicals, Osaka, Japan) was reacted (37°C; 15 min) in kit supplied buffer with RNase inhibitor to remove the cap structure of complete mRNAs. After phenol/chloroform extraction and ethanol precipitation, ligation reaction was carried with T4 RNA ligase (Takara) and 0.5 μg of 5′-adapter RNA oligonucleotide to obtain the oligonucleotide composed by mRNAs attached with 5′-adapter RNA oligonucleotide at 5′ ends that originally had the cap structure. After unligated 5′-adapter oligonucleotide was removed by repeating ethanol precipitation with high salt concentration, reverse transcription reaction was performed using ReverTra Ace (Toyobo) with antisense primer of $P2X_2$ mRNA, which was designed from +531 of NM_053656, and PCR was carried out with obtained cDNAs and primers for adapter and $P2X_2$ mRNA sequence, which were designed to cross the border of exons 1 and 2. The reaction mixture was electrophoresed in agarose gel, and all of amplicon was gel extracted and restricted by XhoI, whose restriction site was designed in adapter sequence. The fragments were cloned into pcDNA3 vector which restricted by XhoI and EcoRV and sequenced. The adapter and primers sequences are as follows. The 5′-adapter RNA oligonucleotide was 5′-GUCUGAGCUCUCGAGAUAGA-3′; the primer for reverse transcription, 5′-GTTGTCAGAAGTTCCATCCTCCAC-3′; the primer for 5′-adapter, 5′-GTCTGAGCTCTCGAGATAGA-3′; and the reverse primer for target amplification, 5′-CGATGAAGACGTACCACACGAA-3′.

Real-Time Quantitative RT-PCR (TaqMan RT-PCR). Retinoids were dissolved in ethanol and added to the culture medium so that the ethanol represented 0.1% of the v/v concentration. Total cellular RNA was prepared using the RNeasy method from QIAGEN (Valencia, CA) according to the manufacturer's instructions and included an on-column DNase I digestion to minimize genomic DNA contamination. The TaqMan One-Step RT-PCR Master Mix Reagent kit (Applied Biosystems, Foster City, CA) was used with each custom designed, gene-specific primer/probe set to amplify and quantify each transcript of interest. Reactions (25 μl) contained 50 ng of total RNA, 200 nM forward and reverse primers, 100 nM TaqMan probe, and RNase Inhibitor Mix in the Master Mix solution. RT-PCR amplification and real-time detection were performed using an ABI PRISM 7700 sequence detection system (Applied Biosystems) for 30 min at 48°C (reverse transcription), 10 min at 95°C (AmpliTaq Gold activation), 38 cycles of denaturation (15 s at 95°C), and annealing/extension (60 s at 60°C). Data were analyzed using ABI Prism Sequence Detection Software, version 1.1. The following primers and probes were used. The TaqMan probe for $P2X_2R$ was 5′-5-carboxy-

fluorescein-CACTACTCCCAGGATCAGCCACCCA-5-carboxytetramethylrhodamine-3'; the forward primer for $P2X_2R$, 5'-CATATCCCTCCCCCACCTA-3'; and the reverse primer, 5'-GTTGGTCCTTCACCTGATGGA-3'. Sense and antisense primers and probes for GAPDH were obtained from Rodent GAPDH Control Reagents (Applied Biosystems).

Plasmids. The 5'-flanking region of *P2rx2* (described above) was inserted into multicloning sites of the pGL3-basic vector (termed pP2X2luc; Promega). The sequence between two KpnI sites (one site is in the multicloning site and other site is at the −1923 position) in the vector was restricted by KpnI (Takara) and ligated to construct a deletion mutant which lacks 501 bp of the 5' end in the pP2X2luc insert (Del-pP2X2luc). The P2X2-GFP vector was a kind gift from Dr. Murrell-Lagnado (Department of Pharmacology, Cambridge University, Cambridge, UK).

Transient Transfections and Luciferase Assays. Transient transfection was carried out with Superfect (QIAGEN) according to the manufacturer's protocol. Fifty percent confluent cells seeded on 48-well plates were transfected with reporter plasmid (pP2X2luc, Del-pP2X2luc, P2X2-GFP). The phRL-TK vector (Promega) was cotransfected to monitor the transfection efficiency. After 48 h incubation, the cells were lysed. Firefly and *Renilla reniformis* luciferase activity were measured by 1420 ARVOsx multilabel counter (PerkinElmer Wallac, Turku, Finland) using a dual-luciferase reporter assay system (Promega). The transfection efficiency was corrected by normalizing the firefly luciferase activity to the *R. reniformis* luciferase activity.

Western Blot of $P2X_2$ Receptor Protein. After treatment of the cells with 9-*cis*-retinoic acid (9-*cis*-RA) for 1 day, the cells were washed with phosphate-buffered saline(−) twice and lysed in buffer containing 10 mM Tris-HCl, pH 7.4, 150 mM NaCl, 10 mM EDTA, 5 mM EGTA, 0.5% mM Nonidet P-40, and 0.5% deoxycholate. The protein concentration was measured by bicinchoninic acid protein assay (Pierce Chemical, Rockford, IL). Proteins (10–30 μg/lane) were mixed with SDS sample buffer, loaded onto a 10% polyacrylamide gel, electrophoresed, and transferred onto a nitrocellulose membrane. The membrane was then blocked in 5% nonfat dry milk in Tris-buffered saline containing 0.1% Tween 20. The membrane was incubated with the anti-rabbit $P2X_2$ polyclonal antibody (1:200; Calbiochem, San Diego, CA) or β-actin (1:5000; Sigma-Aldrich, St. Louis, MO) overnight at 4°C, followed by incubation with the horseradish peroxidase-conjugated anti-rabbit antibody (1:2000; GE Healthcare, Little Chalfont, Buckinghamshire, UK). The blots were probed with an ECL Western blot detection system (GE Healthcare). Quantification of immunoreactive bands was performed by scanned image analysis on a computer.

Whole Cell Patch-Clamp Recording. The cells were placed in a recording chamber and continuously superfused at room temperature (22–24°C) in an extracellular solution containing 140 mM NaCl, 5.4 mM KCl, 1.8 mM $CaCl_2$, 1.0 mM $MgCl_2$, 11.1 mM D-glucose, and 10 mM HEPES; pH adjusted to 7.4 with NaOH. Patch pipettes were filled with an intracellular solution containing 150 mM CsCl, 10 mM HEPES, and 5 mM EGTA; pH adjusted to 7.3 with CsOH. With this solution, patch electrode resistances ranged between 5 and 8 MΩ. The whole cell patch-clamp was made, and cells were voltage-clamped at −60 mV. ATP was diluted with extracellular solution and applied to the patched cell by gravity from a tube (300-μm inner diameter) attached to an electrically controlled valve. Currents were recorded with an Axopatch 200-B amplifier (Molecular Devices, Sunnyvale, CA) and analyzed using pClamp5 software (Molecular Devices).

Measurement of DA Released from PC-12 Cells. Cells were plated on 35-mm dishes and washed twice with 1 ml of balanced salt solution (BSS) containing 150 mM NaCl, 5 mM KCl, 1.2 mM $CaCl_2$, 1.2 mM $MgCl_2$, 25 mM HEPES, and 10 mM D-glucose and then incubated for 1 h with 1 ml of BSS at room temperature. The cells were again washed with BSS and then stimulated by BSS with or without 30 μM ATP for 1 min. BSS was collected in 1.5-ml tubes loaded with 250 μl of 1 N perchloric acid (PCA), and 1 ml of 0.2 N PCA was added to the dishes and incubated for 2 h on ice. Both the collected PCA solutions were centrifuged, and then the supernatants were used for DA measurement. The amount of DA in the solution was measured using high-performance liquid chromatography combined with electrochemical detection.

Intracellular Calcium Imaging. The increase in $[Ca^{2+}]_i$ in single cells was measured by the fura-2 method with minor modifications. Cells were washed with BSS and incubated with 10 μM fura-2 acetoxymethyl ester at 37°C in BSS for 45 min. The coverslips were mounted on an inverted epifluorescence microscope (TMD-300; Nikon, Tokyo, Japan) equipped with a 75-W xenon lamp and band-pass filters of 340-nm wavelength for measurement of the Ca^{2+}-dependent signal (F_{340}) and 360-nm wavelength for measurement of the Ca^{2+}-independent signal (F_{360}).

Results

Homology Search for Transcription Factor Binding Sites in the 5'-Flanking Region of *P2rx2*. The *P2rx2* is located at rat chromosome 12 and has 11 exons between 5'- and 3'-untranslated region (National Center for Biotechnology Information Entrez GeneID 114115). $P2X_2$ mRNA sequence has been first determined by Brake et al. (1994). Of 11 splicing variants registered in GenBank database, only two variants are reported to express functional channel (*P2rx2*, NM_053656; *P2X 2b*, Y10473). The information of the 5'-flanking region of the rat *P2rx2* was obtained from National Center for Biotechnology Information Rat Genome Resources. In the *Rattus norvegicus* (Norway rat) chromosome 12 genomic contig from whole genome shotgun sequence (NW_047378), putative transcription start site of *P2rx2* is predicted by searching the sequence location of rat $P2X_2$ mRNA (NM_053656) using BLAST. Then, a 2524-bp fragment upstream of the Wistar rat *P2rx2* was cloned in the pGL3 vector. Whether the cloned sequence is located in the 5'-flanking region of *P2rx2* is confirmed by sequencing the 743-bp amplicon obtained by genome PCR using specific primers for the third exon of *P2rx2* and our cloned sequence. The homology between database sequence and the cloned sequence was more than 99.8% match. In the cloned sequence, we found three putative RAREs that conformed with a general canonical sequence in which two directly repeated hexanucleotide motifs [consensus (A/G)G(G/T)TCA] are separated by one (DR1: −2309/−2321), four (DR4: −2299/−2314), and five nucleotides (DR5: −2408/−2424) (Fig. 1). We used TESS to verify these sites and confirmed that they were predicted as RAREs. The sequence analysis using TESS also predicted the presence of many consensus sequences for various transcription factors in the cloned fragment such as simian virus 40 protein 1 (Sp-1), AP-1, AP-2, GATA-1, nuclear factor-κB, and cAMP response element-binding protein binding motifs. Sequence data from the 5'-flanking region of the Wistar rat *P2rx2* have been deposited in GenBank with the accession number AY749416. Furthermore using oligo-capping 5' RACE, we could obtain single sequence that encodes 5' region of $P2X_2$ mRNA, suggesting that transcription starting site of *P2rx2* in PC-12 cells is located in 27 bases upstream of RefSeq sequence (NM_053656). Consensus sequences of GC-box (GGGCGG) and initiator (YYANWYY), which are expected to form core promoter region, were found in −67 and −52 bp upstream of transcription starting site determined with oligo-capping 5' RACE.